Lipid droplets are required for lipid mediator production and cancer cell proliferation

Eva Jarc Jovičić[1,2], Anja Pucer Janež[1,2], Thomas O. Eichmann[3,4], Vesna Brglez[1,2], Paul M. Jordan[5], Jana Gerstmeier[5], Gérard Lambeau[6], Oliver Werz[5], Robert Zimmermann[3,7], and Toni Petan[1,*]

[1]Department of Molecular and Biomedical Sciences, Jožef Stefan Institute, Ljubljana, Slovenia
[2]Jožef Stefan International Postgraduate School, Ljubljana, Slovenia
[3]Institute of Molecular Biosciences, University of Graz, Graz, Austria
[4]Center for Explorative Lipidomics, BioTechMed-Graz, Graz, Austria
[5]Department of Pharmaceutical/Medicinal Chemistry, Institute of Pharmacy, Friedrich Schiller University Jena, Jena, Germany
[6]Université Côte d'Azur (UCA), Centre National de la Recherche Scientifique (CNRS), Institut de Pharmacologie Moléculaire et Cellulaire (IPMC), UMR7275, Valbonne Sophia Antipolis, France
[7]BioTechMed-Graz, University of Graz, Graz, Austria

Running title: Lipid droplets and lipid mediators

*To whom correspondence should be addressed:
Toni Petan
Department of Molecular and Biomedical Sciences
Jožef Stefan Institute
Jamova cesta 39
SI-1000 Ljubljana
Slovenia
Tel: +386-1-4773713
Fax: +386-1-4773984
E-mail: toni.petan@ijs.si

Abstract

Lipid droplets are dynamic organelles with a central role in fatty acid metabolism. They protect cells from lipotoxicity by sequestering excess fatty acids but also provide fatty acids for metabolic reactions and signalling events. Here we show that lipid droplet turnover in cancer cells is required for production of ω-3 and ω-6 polyunsaturated fatty acid (PUFA)-derived inflammatory lipid mediators, including eicosanoids and specialised pro-resolving mediators. We show that incorporation of PUFAs into triglycerides mediated by diacylglycerol acyltransferase 1 (DGAT1), and their release by adipose triglyceride lipase (ATGL), are required for cyclooxygenase- and lipoxygenase-dependent lipid mediator production and cancer cell proliferation. The human group X secreted phospholipase A_2 (hGX sPLA$_2$) drives the delivery of membrane-derived PUFAs into lipid droplets, while ATGL promotes the incorporation of lipid droplet-derived PUFAs into phospholipids. The group IVA cytosolic PLA$_2$ (cPLA$_2$α) acts on membrane phospholipids and complements ATGL in the regulation of PUFA trafficking between phospholipids and triglycerides. This study identifies lipid droplets as essential cellular hubs that control PUFA availability for production of lipid mediators involved in inflammation and tumorigenesis.

Keywords: lipid droplets, diacylglycerol acyltransferase, adipose triglyceride lipase, phospholipase A_2, eicosanoids, cancer

Synopsis

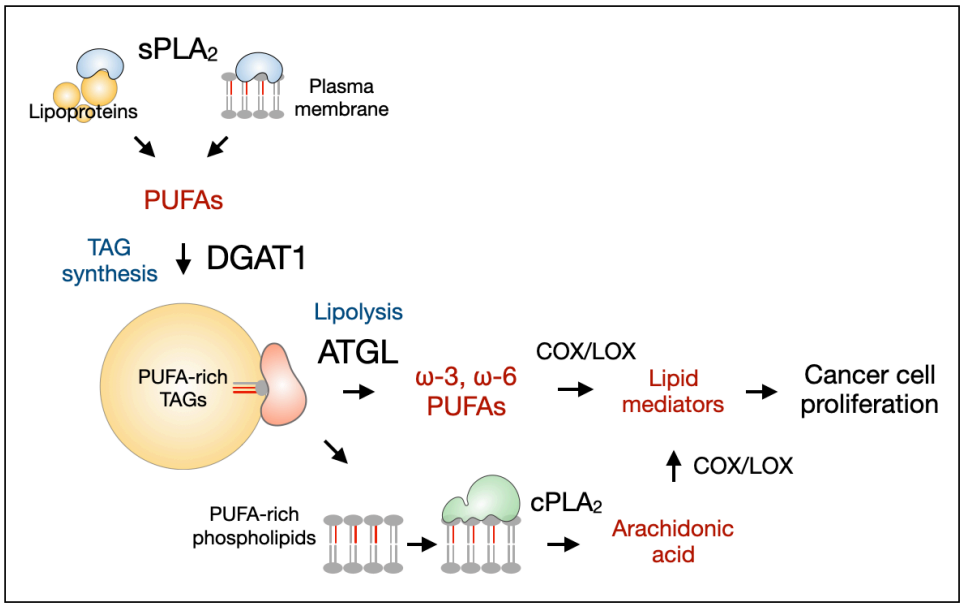

This study shows that lipid droplets in cancer cells control the supply of ω-3 and ω-6 polyunsaturated fatty acids (PUFAs) for the production of lipid mediators, which in turn drive cancer cell proliferation. The esterification of PUFAs into triacylglycerols (TAGs) and their release from lipid droplets are necessary for PUFA entry into lipid mediator production pathways.

- Lipid mediator production induced by the human group X secreted phospholipase A_2 (hGX sPLA2), which releases PUFAs from the plasma membrane and serum lipoproteins, depends on diacylglycerol acyltransferase 1 (DGAT1)-mediated TAG synthesis.
- Adipose triglyceride lipase (ATGL) liberates ω-3 and ω-6 PUFAs from TAGs and drives lipid mediator production via cyclooxygenase (COX) and lipoxygenase (LOX) pathways.
- ATGL promotes the incorporation of lipid droplet-derived PUFAs into phospholipids, which are targeted by the group IVA cytosolic PLA_2 ($cPLA_2\alpha$), thereby selectively supplying arachidonic acid for lipid mediator production.
- Lipid droplets are required for $cPLA_2\alpha$-induced lipid mediator production also in cells that do not depend on ATGL for the supply PUFAs into lipid mediator pathways.

Introduction

Fatty acids (FAs) are universal energy sources and membrane building blocks that are essential for cell growth and proliferation. FAs also stimulate signalling pathways involved in tumour initiation and progression (Röhrig & Schulze, 2016). Cancer cells use various strategies to satisfy their increased needs for FAs, which include reprogramming of FA metabolism (Pavlova & Thompson, 2016; Röhrig & Schulze, 2016) and elevated lipid storage within cytosolic lipid droplets (Olzmann & Carvalho, 2019; Petan, 2020). Lipid droplets are dynamic organelles that transiently store FAs and other lipids in their inert, esterified forms (Krahmer *et al*, 2013; Welte & Gould, 2017; Henne *et al*, 2018). Cancer cells use lipid droplets to maintain their energy and redox homeostasis, and to support membrane synthesis and preserve organelle integrity (Koizume & Miyagi, 2016; Cruz *et al*, 2020; Petan, 2020). Recent studies have also suggested the involvement of lipid droplets in various aspects of inflammation and immunity (Brok *et al*, 2018; Pereira-Dutra *et al*, 2019; Jarc & Petan, 2020; Bosch *et al*, 2021).

Lipid droplets consist of a neutral lipid core that primarily contains triglycerides (TAGs) and sterol esters, and is surrounded by a single layer of phospholipids, wherein numerous proteins are embedded (Olzmann & Carvalho, 2019). Lipid droplets are assembled at the endoplasmic reticulum (ER), where *de novo* synthesized neutral lipids are packaged into nascent lipid droplets that bud from the ER membrane (Walther *et al*, 2017; Thiam & Ikonen, 2020). TAG biosynthesis, catalysed by diacylglycerol acyltransferases 1 and 2 (DGAT1, 2), protects cells and tissues against lipotoxicity by sequestering excess FAs (Listenberger *et al*, 2003; Bailey *et al*, 2015; Nguyen *et al*, 2017; Jarc *et al*, 2018), and reduces diet-induced insulin resistance and inflammation (Koliwad *et al*, 2010; Greenberg *et al*, 2011). However, recent studies have suggested that DGAT1-dependent lipid droplet formation is exploited by cancer cells for the prevention of oxidative damage and organelle dysfunction, thereby supporting cancer cell survival and tumour growth (Ackerman *et al*, 2018; Jarc *et al*, 2018; Cheng *et al*, 2020; preprint: Wilcock *et al*, 2020; Dierge *et al*, 2021).

Lipid droplet breakdown occurs via either lipolysis, which is initiated by adipose TAG lipase (ATGL), or lipophagy, which is a selective form of autophagy (Zechner *et al*, 2017). ATGL is the major cytosolic neutral TAG hydrolase in mammalian cells. Its activity is crucial for mobilisation of TAG reserves from adipose tissue, and for energy production during fasting and exercise (Zimmermann *et al*, 2004; Zechner *et al*, 2012). At the cellular level, ATGL promotes FA transfer from lipid droplets to mitochondria and fuels oxidative metabolism (Smirnova *et al*, 2005; Haemmerle *et al*, 2011; Rambold *et al*, 2015). Furthermore, ATGL regulates signalling pathways that coordinate metabolism, stress responses and inflammation (Schweiger *et al*, 2017; Zechner *et al*, 2017; Jarc & Petan, 2020). Several reports have shown

that ATGL can support tumour growth (Nieman *et al*, 2010; Zagani *et al*, 2015; Wang *et al*, 2017; Yin *et al*, 2021), but a tumour-suppressor role for ATGL has also been suggested (Al-Zoughbi *et al*, 2016).

The oxygenation of ω-6 and ω-3 polyunsaturated FAs (PUFAs) by cyclooxygenases (COXs), lipoxygenases (LOXs) and CYP450 epoxygenases leads to the production of several families of bioactive lipid mediators that collectively modulate inflammatory and immune responses (Serhan, 2014; Dennis & Norris, 2015). Eicosanoids, derived from the ω-6 PUFA arachidonic acid (C20:4n-6; AA), have been shown to promote tumour growth (Wang & DuBois, 2010; Greene *et al*, 2011), whereas the ω-3 PUFA-derived resolvins suppress tumour-associated inflammation and reduce tumour growth (Sulciner *et al*, 2018; Fishbein *et al*, 2020). The compositions of the lipid mediator mixtures released from cells are dictated by the availability of particular PUFAs for lipid mediator-producing enzymes (Wang & DuBois, 2010; Greene *et al*, 2011; Jarc & Petan, 2020). However, our current understanding of the control of PUFA supply for lipid mediator production is poor, particularly as this is intrinsically dependent on the complex control of cellular (PU)FA metabolism, which includes their uptake, synthesis, storage, breakdown, remodelling and trafficking between different lipid pools (Pérez-Chacón *et al*, 2009; Serhan, 2014; Astudillo *et al*, 2019; Jarc & Petan, 2020).

The canonical pathway that supplies AA for eicosanoid production depends on group IVA cytosolic phospholipase A_2 (cPLA$_2$α). cPLA$_2$α has long been known to be the major PLA$_2$ involved in stimulus-induced eicosanoid production and promotion of inflammation in various pathophysiological settings (Bonventre *et al*, 2004; Shimizu, 2009; Murakami *et al*, 2011; Leslie, 2015). Upon cell activation, cPLA$_2$α binds to perinuclear membranes of the ER and Golgi complex and selectively hydrolyses phospholipids containing AA at the *sn*-2 position (Hayashi *et al*, 2021). Numerous other members of the PLA$_2$ superfamily also promote lipid mediator production, either through activation of cPLA$_2$α or by acting independently on their respective phospholipid pools, thereby also releasing PUFAs other than AA (Saiga *et al*, 2005; Duchez *et al*, 2019; Astudillo *et al*, 2019). In particular, several secreted PLA$_2$s (sPLA$_2$s) have been implicated in the production of eicosanoids and ω-3 PUFA-derived specialised pro-resolving mediators (Mounier *et al*, 2004; Surrel *et al*, 2009; Murakami, 2017; Sato *et al*, 2020).

Among mammalian sPLA$_2$s, the group X sPLA$_2$ is the most potent enzyme at hydrolysing phosphatidylcholine-rich membranes, including the plasma membrane of mammalian cells and lipoproteins (Lambeau & Gelb, 2008). Group X sPLA$_2$ can release various unsaturated FAs, including ω-3 and ω-6 PUFAs, and it is involved in inflammation, immunity, adipogenesis and tumorigenesis (Li *et al*, 2010; Ait-Oufella *et al*, 2013; Murase *et al*, 2016; Murakami, 2017; Ogden *et al*, 2020). It can induce colon cancer cell proliferation through production of eicosanoids and other lipid mediators (Surrel *et al*, 2009; Schewe *et al*, 2016). Our previous studies have shown that human group X (hGX) sPLA$_2$ stimulates lipid

droplet biogenesis in breast cancer cells, which is associated with increased cell proliferation and resistance to starvation-induced stress (Pucer *et al*, 2013). In breast cancer cells exposed to excess PUFAs, hGX sPLA$_2$ modulates unsaturated FA trafficking and lipid droplet turnover, thus protecting from oxidative stress and cell death (Jarc *et al*, 2018). Other PLA$_2$s, including cPLA$_2$α, also influence lipid droplet metabolism, although the potential links between various PLA$_2$s, lipid droplets and lipid mediator production have been poorly explored to date (Guijas *et al*, 2014; Jarc & Petan, 2020).

Recent evidence has suggested that besides membrane phospholipids, other lipid pools can also provide PUFAs for lipid mediator production (Jarc & Petan, 2020). This includes neutral lipids that are stored within lipoproteins and lipid droplets (Dichlberger *et al*, 2014; Schlager *et al*, 2015, 2017). Lipid droplets in immune cells have been implicated in AA trafficking and inflammatory responses (Dvorak *et al*, 1983; Triggiani *et al*, 1994; Bozza *et al*, 2011). Furthermore, several eicosanoid biosynthetic enzymes localise to lipid droplets, which suggests that lipid droplet-derived fatty acids can participate in eicosanoid production (Accioly *et al*, 2008). In agreement with this, ATGL- and hormone-sensitive lipase (HSL)-mediated lipolysis have been shown to participate in eicosanoid production in mast cells, neutrophils and adipocytes (Dichlberger *et al*, 2014; Schlager *et al*, 2015; Gartung *et al*, 2016; Sohn *et al*, 2018). In addition, monoacylglycerol lipase, which acts on monoglycerides derived from TAG lipolysis or phospholipid hydrolysis, has been shown to promote tumorigenesis through the dual control of endocannabinoid removal and eicosanoid production (Nomura *et al*, 2010, 2011). Most notably, ATGL deficiency has been shown to reduce PUFA availability for lipid mediator production and enhance neutrophil immune responses *in vivo* (Schlager *et al*, 2015). Whether ATGL has a similar role in cancer cells is not known. It is also not clear whether lipid droplets merely act as optional and transient storage sites for PUFAs, or whether they are *de-facto* required for lipid mediator production.

Lipid droplets are emerging as modulators of the subcellular distribution of mono-unsaturated FAs (MUFAs) and PUFAs, which is important for various cellular responses to stress and for determination of cell fate (Bailey *et al*, 2015; Ackerman *et al*, 2018; Jarc *et al*, 2018; Dierge *et al*, 2021). Here, we investigated whether lipid droplets can influence the delivery of PUFAs into the oxygenation pathways that are responsible for regulated production of lipid mediators. We examined how DGAT and ATGL affect lipid mediator production in cancer cells, and how they cooperate with different PLA$_2$ enzymes in the control of PUFA trafficking between membrane phospholipids and TAGs. We show that incorporation of PUFAs into TAGs and their subsequent release via lipolysis are essential for the production of various lipid mediators, and that this process is linked to cancer cell proliferation.

Results

Membrane phospholipid hydrolysis by hGX sPLA$_2$ leads to enrichment of lipid droplets with long-chain PUFA-TAGs

We have shown previously that hGX sPLA$_2$ stimulates TAG synthesis and induces lipid droplet accumulation in several breast cancer cell lines, including the highly invasive and metastatic triple-negative MDA-MB-231 cells (Pucer *et al*, 2013; Jarc *et al*, 2018). To determine whether this extends to other cancer cell types, a panel of cancer cell lines was treated with 10 nM recombinant hGX sPLA$_2$ and changes in lipid droplet levels were quantified using flow cytometry, and visualised using confocal microscopy. hGX sPLA$_2$ stimulated lipid droplet accumulation in the majority of these cancer cell lines, including neuroblastoma, prostate, colorectal, ovarian and lung cancer cell lines (Fig. 1A, B). An increase in neutral lipid accumulation was also seen for several immortalised non-tumorigenic cell lines (Fig. 1A). Of note, there was a reduction in lipid droplet content and TAG levels upon hGX sPLA$_2$ treatment only in the HeLa cervical cancer cells (Appendix Fig. S1A). Therefore, hGX sPLA$_2$ is a potent stimulator of lipid droplet turnover, the activity of which in most cell types, but not all, leads to a net increase in lipid droplet accumulation.

We have previously reported that hGX sPLA$_2$ hydrolyses membrane phospholipids in intact MDA-MB-231 breast cancer cells to release various unsaturated FAs, including primarily oleic acid (C18:1n–9; OA), plus significant amounts of ω-3 and ω-6 PUFAs (Jarc *et al*, 2018). Furthermore, hGX sPLA$_2$ induces significant TAG acyl-chain remodelling in MDA-MB-231 cells exposed to excess exogenous docosahexaenoic acid (C22:6n–3; DHA), thereby increasing the levels of MUFAs esterified in lipid droplet-stored TAGs (Jarc *et al*, 2018). To support the idea that FAs released from MDA-MB-231 cell membrane phospholipids by hGX sPLA$_2$ are incorporated into growing lipid droplets (Fig. 1C), we examined the effects of hGX sPLA$_2$ on the incorporation of radiolabelled [^{14}C]-OA into cellular lipids (Appendix Fig. S1B). Thin-layer chromatography (TLC) analysis revealed that the hGX sPLA$_2$ treatments increased the amounts of [^{14}C]-OA that were esterified in TAG species in MDA-MB-231 cells grown under serum-rich conditions (Fig. 1D; Appendix Fig. S1C). This enrichment of TAGs with OA persisted after removal of hGX sPLA$_2$ and during prolonged periods of serum starvation. As hGX sPLA$_2$ acts on both serum lipoproteins and intact adherent cells (Guillaume *et al*, 2015; Jarc *et al*, 2018), it is possible that the FA flux from either or both of these lipid pools supported the lipid droplet biogenesis. As the hGX PLA$_2$ induction of OA incorporation into TAGs was not abolished during treatments in the absence of serum (Fig. 1D; Appendix Fig. S1C), this confirmed a direct action of hGX sPLA$_2$ on the cancer cells to drive the incorporation of cell-

membrane-derived OA into TAGs, and thus to induce long-lasting changes in the TAG acyl-chain composition.

To determine the full extent of TAG remodelling induced by hGX $sPLA_2$, we performed lipidomic analysis of untreated and hGX-$sPLA_2$-treated MDA-MB-231 cells grown in the presence and absence of serum (Fig. 1E–K; Appendix Fig. S1D, E). As expected, a significant increase in the total amount of TAGs was observed in the hGX-$sPLA_2$-treated cells grown under both conditions (Fig. 1F). Both serum-fed (Fig. 1G, H) and serum-starved (Fig. 1I) cells treated with hGX $sPLA_2$ had elevated levels of long-chain and highly unsaturated TAG species. Significant changes were observed in TAG species of at least 60 C-atoms (Fig. 1J) and more than seven double bonds (Fig. 1K), such as 58:8, 58:9, 60:8, 60:9, 62:10, 62:12 and 64:12 (Appendix Fig. S1D, E). On the other hand, there was a significant reduction in the abundance of shorter-chain saturated and weakly unsaturated TAG species; i.e., those with 52 or less C-atoms (Fig. 1J) and containing exclusively saturated or only one mono-unsaturated acyl chain (Fig. 1K). Therefore, the lipid droplets in breast cancer cells treated with hGX $sPLA_2$ are significantly enriched with PUFA-containing TAG species.

ATGL-mediated lipid droplet breakdown is required for PGE_2 production in serum-starved cancer cells

Serum withdrawal induces lipid droplet breakdown in most cell types (Bosch *et al*, 2020). Given the hGX-$sPLA_2$-induced enrichment of lipid droplets with PUFAs, we hypothesised that starvation-induced lipid droplet breakdown provides PUFAs for lipid mediator production. To find out if the breakdown of PUFA-rich lipid droplets facilitates eicosanoid production in cancer cells, lipid droplet biogenesis was first stimulated with hGX $sPLA_2$ or with exogenous AA in serum-rich medium (Fig. 2A). Then the cells were serum-starved in the absence of these stimuli to induce lipid droplet breakdown (Fig. EV1A, B) and quantify the release of glycerol, an indicator of TAG lipolysis, and the production of prostaglandin (PG)E_2, a major inflammation- and cancer-related eicosanoid. Serum-starved MDA-MB-231, HeLa and A549 cancer cells pre-treated with hGX $sPLA_2$ released more glycerol (Fig. EV1C) and produced more PGE_2 than control untreated cells (Fig. 2B). Accordingly, hGX-$sPLA_2$-treated MDA-MB-231 and A549 cells had more lipid droplets at the beginning of the starvation and a greater proportion of these lipid droplets were broken down during the starvation (Fig. EV1A, B). Although HeLa cells treated with hGX $sPLA_2$ showed a net reduction in neutral lipid levels (Fig. EV1A), during serum starvation they still released more glycerol (Fig. EV1F) and produced more PGE_2 (Fig. 2B) than the untreated cells. MDA-MB-231 and HeLa cells pre-treated with exogenous AA also increased their production of PGE_2 during starvation (Fig. EV1D). Together with the observed hGX-$sPLA_2$-induced PUFA-TAG enrichment of lipid droplets, the elevated

lipid droplet turnover, lipolytic activity and PGE_2 production in hGX-$sPLA_2$-treated cells suggest that lipid droplet breakdown drives PGE_2 synthesis in serum-starved cancer cells.

Recent evidence has suggested that TAG lipolysis mediated by ATGL contributes to the production of lipid mediators in endothelial and immune cells (Dichlberger *et al*, 2014; Schlager *et al*, 2015; Riederer *et al*, 2017). Here we asked whether lipid droplet breakdown via ATGL is required for lipid mediator production in serum-starved cancer cells, and whether it mediates hGX-$sPLA_2$-stimulated PGE_2 synthesis. ATGL-specific siRNAs were used to suppress ATGL expression in cancer cells exposed to nutrient-rich conditions, followed by serum starvation (Fig. 2C; Fig. EV1E). The deficiency of ATGL augmented lipid droplet levels under both serum-rich and serum-starvation conditions (Fig. 2D, F; Fig. EV1F, H, I, K). Importantly, ATGL depletion reduced basal PGE_2 production in serum-starved untreated MDA-MB-231 and HeLa cells, and fully blocked hGX-$sPLA_2$-induced PGE_2 production in these two cell lines (Fig. 2E; Fig. EV1G). ATGL silencing also attenuated lipid droplet breakdown and suppressed the production of PGE_2 in MDA-MB-231 cells pre-treated with exogenous AA (Fig. EV1L, M). However, ATGL deficiency did not suppress the basal or hGX-$sPLA_2$-induced PGE_2 production in the A549 cells, and even resulted in a slight increase in PGE_2 levels (Fig. EV1J). Furthermore, in contrast to MDA-MB-231 and HeLa cells, where ATGL deficiency suppressed glycerol release, ATGL depletion in A549 cells augmented hGX-$sPLA_2$-induced glycerol release (Fig. EV1N, O).

To support these findings, we next asked whether ATGL overexpression leads to increased lipolysis and PGE_2 production in the breast and cervical cancer cells (Fig. 2G). Here, ectopic ATGL expression stimulated glycerol release (Fig. 2H; Fig. EV1P) without having any significant effects on the total neutral lipid levels (Fig. EV1R). Both untreated and $sPLA_2$-treated ATGL-overexpressing cells produced significantly more PGE_2 during starvation (Fig. 2I). The increase in lipolytic glycerol release and PGE_2 production induced by ATGL overexpression was fully reversed in the presence of ATGL-specific siRNA in both of these cell lines (Fig. 2H, I), which confirmed the specificity of the effect of ATGL overexpression. Collectively, these data suggested that lipid droplet breakdown via ATGL is required for basal, AA-induced and hGX-$sPLA_2$-stimulated PGE_2 production in serum-starved MDA-MB-231 breast and HeLa cervical cancer cells, but not in A549 lung cancer cells (Fig. 2J).

ATGL-mediated lipid droplet breakdown drives production of eicosanoids and specialised pro-resolving mediators

The data presented above demonstrate that transient storage of AA within lipid droplet TAGs followed by AA release from TAGs by ATGL are intermediate steps in basal and hGX-$sPLA_2$-stimulated production of PGE_2, a major pro-inflammatory and pro-tumorigenic AA-derived eicosanoid. To find out if ATGL-mediated TAG lipolysis promotes the production of a wider

range of eicosanoids and related lipid mediators (which might also derive from other PUFAs), we performed targeted liquid chromatography-tandem mass spectrometry-based metabololipidomics to examine the effects of ATGL silencing on the lipid mediator profiles of untreated and hGX-sPLA$_2$-treated breast cancer cells. Here, pre-treatment of breast cancer cells with hGX sPLA$_2$, which enriches PUFA-TAGs in lipid droplets, stimulated the starvation-induced production of various lipid mediators, biosynthesised from different PUFAs by various enzymatic pathways, including prostaglandins, specialized pro-resolving mediators and numerous hydroxylated PUFAs (Fig. 3A–C). We quantified 34 different lipid mediators with 18 lipid mediator species that were elevated in cells pre-treated with hGX sPLA$_2$ (Fig. 3A–C; Appendix Fig. S2). hGX sPLA$_2$ promoted the synthesis of eicosapentaenoic acid (EPA)-derived lipid mediators (6/6 species), as well as the production of AA-derived (5/13 species) and DHA-derived (7/15 species) products (Fig. 3B, C; Appendix Fig. S2). Importantly, ATGL depletion suppressed the release of all of the hGX-sPLA$_2$-induced lipid mediators. Furthermore, ATGL silencing strongly inhibited the basal, hGX-sPLA$_2$-independent production of numerous lipid mediators, including PGE$_2$ (Fig. 3B, C; Appendix Fig. S2). Cells pre-treated with hGX sPLA$_2$ under serum-fed conditions also released significantly more unesterified PUFAs, including AA, EPA and DHA, during the following serum starvation, which was prevented by ATGL silencing (Fig. 3D). This suggested that a significant portion of hGX sPLA$_2$-released PUFAs is not used for lipid mediator production and that these “excess” membrane-derived PUFAs still undergo a cycle of esterification into TAGs and release from TAGs by ATGL. Therefore, lipid droplets drive starvation-induced production by cancer cells of a wide spectrum of lipid mediators that are derived from PUFAs stored within TAGs and are released by ATGL-mediated lipolysis (Fig. 3E).

Cancer cells depleted of lipid droplets have impaired PGE$_2$ production

The data presented above demonstrate that lipid droplets and ATGL-mediated lipolysis promote the entry of exogenously added and hGX-sPLA$_2$-derived PUFAs into lipid mediator production pathways in serum-starved cancer cells. To determine whether the incorporation of PUFAs into TAGs is indeed a prerequisite for PUFA use as substrates for lipid mediator biosynthesis, DGAT-mediated TAG synthesis was inhibited using a combination of specific inhibitors of DGAT1 and DGAT2 (DGATi), T863 and PF-06424439, and changes in lipid droplet turnover and PGE$_2$ release were examined. DGAT inhibition during serum feeding strongly suppressed basal, hGX-sPLA$_2$-induced and exogenous AA-induced lipid droplet accumulation (Fig. 4A, B, D). There was an almost complete depletion of lipid droplets in serum-fed DGATi-treated cells (Fig. 4B), which allowed only a minimal residual lipid droplet breakdown during the subsequent serum starvation (Fig. 4A). Importantly, cancer cells depleted of lipid droplets did not produce eicosanoids during serum starvation, showing low basal PGE$_2$ release and no

increase in PGE_2 production upon stimulation with either hGX $sPLA_2$ or AA (Fig. 4C, E). DGAT inhibition also abolished PGE_2 production in A549 lung cancer cells (Fig. 4C), whereas ATGL depletion failed to do so (Fig. EV1J), suggesting a role of lipid droplets in eicosanoid production in A549 lung cancer cells as well. Therefore, DGAT-mediated TAG biosynthesis under serum-rich conditions is a prerequisite for lipid mediator production in serum-starved cancer cells.

Serum removal induces strong activation of *de-novo* lipogenesis in MDA-MB-231 cells (Pucer *et al*, 2013), and treatment of serum-starved cells with hGX $sPLA_2$ resulted in a net increase in TAG levels (Fig. 1F). To examine whether TAG synthesis during serum starvation has a role in eicosanoid production, control and ATGL-depleted cells were treated with DGATi during serum feeding or during serum starvation. As expected, DGAT inhibition during serum feeding abolished both hGX-$sPLA_2$-stimulated and ATGL-depletion-induced changes in lipid droplet accumulation in MDA-MB-231 and HeLa cells (Fig. EV2A). In contrast, DGAT inhibition during serum starvation did not significantly affect lipid droplet levels in these two cell lines (Fig. 4F; Fig. EV2B), nor did it affect PGE_2 release in MDA-MB-231 cells (Fig. 4F). However, DGAT inhibition in serum-starved A549 cells reduced lipid droplet abundance and suppressed PGE_2 production, both in control and in ATGL-deficient cells (Fig. 4G). This suggested that during serum starvation significant TAG biosynthesis occurred in A549 cells and contributed to eicosanoid production, via ATGL-independent mechanisms. Accordingly, in A549 cells, DGAT inhibition during both serum feeding and starvation was necessary for full suppression of PGE_2 production (Fig. EV2C). These data demonstrate that serum-starvation-induced TAG synthesis contributes to eicosanoid production in A549 cells, but not in the breast and cervical cancer cells.

In summary, while the breakdown of pre-existing DGAT-induced lipid droplets is the predominant mechanism of lipid droplet-driven eicosanoid production in the serum-starved breast and cervical cancer cells, A549 lung cancer cells also employ starvation-induced TAG synthesis to support eicosanoid production.

$cPLA_2\alpha$ cooperates with ATGL and depends on lipid droplet turnover to drive eicosanoid production

Given the well-accepted role of $cPLA_2\alpha$ in providing AA for eicosanoid biosynthesis, we next asked whether $cPLA_2\alpha$ participates in lipid droplet-driven lipid mediator production in serum-starved cancer cells. We speculated that, in principle, $cPLA_2\alpha$ might cooperate with ATGL to provide AA for eicosanoid release via at least three possible mechanisms (Fig. 5A): (a) ATGL-mediated transfer of TAG-derived AA into phospholipid pools that are then targeted by $cPLA_2\alpha$; (b) $cPLA_2\alpha$-induced incorporation of phospholipid-derived AA into TAGs, followed by AA release by ATGL; or (c) independent actions of $cPLA_2\alpha$ and ATGL on their respective lipid pools.

To examine these hypotheses, we first used siRNAs to deplete cancer cells of cPLA$_2$α alone or in combination with ATGL (Fig. 5B; Fig. EV3A, B), and measured lipid droplet levels and PGE$_2$ release. cPLA$_2$α-depleted cells showed slightly higher levels of neutral lipids during serum feeding (Fig. EV3C) and this effect persisted during the subsequent serum starvation (Fig. 5B), being particularly evident in starving MDA-MB-231 and A549 cells pre-treated with hGX sPLA$_2$. Moreover, in all three cell lines, silencing of both cPLA$_2$α and ATGL potentiated the enhancing effects of individual depletion on neutral lipid accumulation (Fig. 5B). Notably, cPLA$_2$α depletion abolished basal and hGX-sPLA$_2$-elicited eicosanoid release in A549 cells (Fig. 5B), while ATGL silencing increased PGE$_2$ production (Figs. 5B, EV1J). On the other hand, cPLA$_2$α knockdown had no effects on eicosanoid production in MDA-MB-231 cells, while ATGL knockdown decreased PGE$_2$ production. Surprisingly, the silencing of cPLA$_2$α in HeLa cells resulted in a marked increase in PGE$_2$ production, which was partially reduced in HeLa cells depleted of both ATGL and cPLA$_2$α (Fig. 5B). These data suggested that cPLA$_2$α modulates lipid droplet turnover in all three cancer cell lines. However, its contribution to PGE$_2$ production is serum-starved cancer cells is cell-type-specific. It appears to be of either a minor importance in MDA-MB-231 breast cancer cells or to have a modulatory role in HeLa cervical cancer cells, whereby both cell types rely on ATGL for PGE$_2$ production. In contrast, in serum-starved A549 cells cPLA$_2$α has a predominant role in PGE$_2$ production.

To find out more about the possible interplay between cPLA$_2$α and ATGL, we asked how reciprocal overexpression of one and silencing of the other might affect lipid droplet turnover and PGE$_2$ production (Fig. 5C). In all three cell lines, the individual overexpression of ATGL or cPLA$_2$α had minimal effects on neutral lipid levels (Fig. EV3D, E). Nevertheless, the overexpression of either ATGL or cPLA$_2$α induced significant increases in PGE$_2$ production, which reached comparable levels in the three cell lines (Fig. 5C). Importantly, ATGL silencing blocked PGE$_2$ production induced by overexpression of cPLA$_2$α in MDA-MB-231 and HeLa cells, whereas cPLA$_2$α silencing only partially reduced eicosanoid production induced by ATGL overexpression in MDA-MB-231 cells, and even increased that in HeLa cells. On the contrary, in A549 cells, ATGL knockdown did not affect cPLA$_2$α-induced PGE$_2$ production, but silencing of cPLA$_2$α reduced PGE$_2$ release from ATGL-overexpressing cells (Fig. 5C). Taken together, these data suggested that ATGL is the main enzyme in the provision of PUFAs for eicosanoid production in MDA-MB-231 and HeLa cells, whereby cPLA$_2$α stimulation of eicosanoid production depends on ATGL. In contrast, in A549 cells, cPLA$_2$α has a dominant role in PGE$_2$ production, which is independent of ATGL, but is still associated with changes in lipid droplet turnover.

To determine whether lipid droplets are required for cPLA$_2$α-driven lipid mediator production, cPLA$_2$α and ATGL were overexpressed in cells depleted of lipid droplets using DGAT inhibitors (Fig. 5D; Fig. EV3F). As expected, TAG synthesis was necessary for ATGL

stimulation of both basal and sPLA$_2$-induced eicosanoid production (Fig. 5D). In all three cell lines, cPLA$_2$α-overexpression-induced eicosanoid production was completely abolished upon depletion of lipid droplets (Fig. 5D). Therefore, lipid droplets are required for both cPLA$_2$α-driven and ATGL-driven lipid mediator production. cPLA$_2$α and ATGL appear to have cell-type-specific roles that are either cooperative or complementary for both lipid droplet turnover and eicosanoid production. In the breast and cervical cancer cells, deficiency of ATGL impairs cPLA$_2$α-induced PGE$_2$ production, which suggests the possibility that the transfer of AA from TAGs to phospholipids is a prerequisite for the action of cPLA$_2$α.

ATGL and cPLA$_2$α have complementary roles in TAG and phospholipid acyl-chain remodelling

To support the finding that cPLA$_2$α affects lipid droplet turnover (Fig. 5B), the changes in lipid droplet morphology in cPLA$_2$α and ATGL single and double knockdown cells were visualised and quantified under the microscope. For ATGL-depleted MDA-MB-231 and HeLa cells, the diameters of the lipid droplets were significantly increased relative to control cells, under both serum-fed and serum-starved conditions (Fig. 6A, B; Fig. EV4A, B). However, ATGL depletion had only a modest effect on the number of lipid droplets per cell (Fig. 6C, D). In serum-starved A549 cells, ATGL silencing reduced the number of lipid droplets per cell, but did not significantly affect the diameter (Fig. 6E; Fig. EV4C, D). Of note, among the three cell lines, A549 cells had the highest number of lipid droplets, which had the greatest diameters and the widest size heterogeneity. Surprisingly, depletion of cPLA$_2$α in all three of these cancer cell lines resulted in more lipid droplets per cell, which was particularly evident in hGX-sPLA$_2$-treated cells (Fig. 6C–E). In most cases, depletion of cPLA$_2$α had no effects on lipid droplet size. In comparison with ATGL-deficient cells, the silencing of both cPLA$_2$α and ATGL led to increased lipid droplet numbers in all of these cell lines, and particularly under serum-starved conditions, which suggested that cPLA$_2$α affects lipid droplet numbers independently of ATGL. Thus, while ATGL predominantly affects lipid droplet size, which is in line with its role in TAG lipolysis, cPLA$_2$α appears to have a modulatory role in lipid droplet turnover, whereby its deficiency leads to a minimal increase in total cellular neutral lipid content and a significant increase in lipid droplet numbers. These effects might be a consequence of the direct or indirect involvement of cPLA$_2$α in the lipid droplet biogenesis and/or breakdown processes.

On the basis that the above data suggested that ATGL is required for cPLA$_2$α-induced eicosanoid production in serum-starved MDA-MB-231 and HeLa cells (Fig. 5C), we speculated that this occurs by ATGL-induced transfer of TAG-derived AA into phospholipid pools that are then targeted by cPLA$_2$α (Fig. EV5A). Additionally, given that cPLA$_2$α has been reported to modulate lipid droplet biogenesis, possibly by inducing changes in the composition of the ER membrane and thereby affecting nascent lipid droplet formation (Guijas *et al*, 2014), we

hypothesised that cPLA$_2$α affects lipid droplet turnover (and thus indirectly impacts upon ATGL-mediated lipolysis) by inducing global changes in the composition of the phospholipid and/or TAG lipid pools. To examine these hypotheses and determine how hGX sPLA$_2$, ATGL and cPLA$_2$α affect PUFA trafficking between the phospholipid and TAG pools during serum starvation in MDA-MB-231 cells, we performed single and double knockdowns followed by lipidomic analyses comparing the lipid compositions of cells first pre-treated with hGX sPLA$_2$ during nutrient sufficiency and subsequently serum-starved for 0 h, 3 h or 24 h (Fig. EV5B).

First, treatment of breast cancer cells with hGX sPLA$_2$ led to PUFA enrichment of both TAGs and phospholipids (Figs. 7A, EV5C; Appendix Fig. S3A). hGX-sPLA$_2$-induced PUFA-TAG enrichment was seen for serum-fed cells (i.e., 0 h serum starvation), and it persisted upon hGX sPLA$_2$ and serum removal. Importantly, the enrichment of phospholipids with PUFA acyl chains progressively increased during the course of serum starvation (Fig. EV5C). By the end of the 24 h of serum starvation, the levels of numerous long-chain PUFA-phosphatidylcholine and several PUFA-phosphatidylinositol and PUFA-phosphatidylethanolamine species were increased. These data suggested that a significant portion of sPLA$_2$-released PUFAs that are incorporated into TAGs in serum-fed cells are gradually released via lipolysis during serum starvation and are re-esterified into phospholipids.

Second, depletion of ATGL increased TAG content across all of the lipid species, and also altered the cellular phospholipid composition (Figs. 7A, EV5C; Appendix Fig. S3A). The effect of ATGL depletion on TAG levels gradually increased during the serum starvation, and was greatest after 24 h without serum (Fig. 7B). Here, numerous PUFA-TAG species were elevated, which confirmed that ATGL hydrolyses PUFA-TAGs during serum starvation. ATGL silencing did not significantly affect the already high PUFA-TAG contents in hGX-sPLA$_2$-treated cells (Fig. 7A), although it increased the levels of some saturated FA (SFA)/MUFA-TAG species (Fig. 7C). The retention of various TAG species within lipid droplets due to ATGL deficiency is in agreement with the general lack of TAG acyl-chain specificity of ATGL (Eichmann *et al*, 2012). Importantly, ATGL deficiency reverted the elevation of PUFA phospholipids induced by hGX sPLA$_2$ and observed in serum-starved cells (Fig. EV5C; Appendix Fig. S3A). This is consistent with a reduced flux of PUFAs from TAGs into phospholipids due to ATGL depletion. A similar, but less apparent, trend towards a decrease in PUFA-phospholipid levels was observed for ATGL-deficient cells that were not treated with hGX sPLA$_2$ (Fig. EV5C). Thus, in serum-starved cancer cells, ATGL hydrolyses various TAG species, including numerous PUFA-TAGs, and provides PUFAs for esterification into phospholipids.

Third, depletion of cPLA$_2$α had a predominant effect on the phospholipids (Fig. 7A; Figs. EV5C; Appendix Fig. S3A), and also affected TAG composition (Fig. 7C). Numerous PUFA-containing phosphatidylcholine and phosphatidylethanolamine species were

progressively elevated in cPLA$_2$α-deficient cells over the course of the serum starvation, in both control and hGX-sPLA$_2$-treated cells (Fig. EV5C), which suggested that these lipids are targeted by cPLA$_2$α during serum starvation. The enrichment of phospholipids with PUFAs as a result of cPLA$_2$α deficiency was more pronounced than that induced by hGX sPLA$_2$ treatment alone (Fig. EV5C; Appendix Fig. S3A). A LION/web lipid ontology analysis suggested that the enrichment of phospholipids with PUFAs in cPLA$_2$α-deficient cells is indicative of significant changes in membrane biophysical properties, including increased lateral diffusion, reduced bilayer thickness and a lower transition temperature (Appendix Figs. S3B, C). Furthermore, in cPLA$_2$α and ATGL double-knockdown cells, the decreased abundance of PUFA-phospholipid species observed in ATGL-deficient cells was reversed (Figs. 7A, EV5D; Appendix Fig. S3A), which suggested the possibility that ATGL-derived PUFAs are incorporated into a phospholipid pool that is targeted by cPLA$_2$α. On the other hand, cPLA$_2$α silencing did not affect hGX-sPLA$_2$-induced PUFA-TAG enrichment (Fig. 7A), which indicated that cPLA$_2$α is not required for incorporation of hGX-sPLA$_2$-released PUFAs into TAGs. However, cPLA$_2$α depletion reduced the content of SFA/MUFA-TAGs in lipid droplets of hGX-sPLA$_2$-treated cells (Fig. 7C). This was fully reversed in the cPLA$_2$α and ATGL double-knockdown cells, which suggested that the effect of cPLA$_2$α depletion on TAG composition depends on ATGL-mediated lipolysis (Fig. 7A, C). Therefore, during cancer cell starvation, ATGL promotes the transfer of PUFAs from TAGs into a phospholipid pool that might be targeted by cPLA$_2$α, but cPLA$_2$α also alters TAG composition in an ATGL-dependent manner.

Collectively, these data suggested that hGX-sPLA$_2$-liberated PUFAs are used for the synthesis of both phospholipids and TAGs, whereby the phospholipids are targeted by cPLA$_2$α and the TAGs are targeted by ATGL, while both cPLA$_2$α and ATGL may also reciprocally modulate these two major lipid pools. At least in MDA-MB-231 cells, hGX-sPLA$_2$-liberated PUFAs are first and predominantly incorporated into TAGs of growing lipid droplets, and are then redistributed into phospholipids upon TAG lipolysis by ATGL, particularly during serum starvation (Fig. 7D). Some of the ATGL-released PUFAs are directly used for eicosanoid production (i.e., independent of cPLA$_2$α), while some are re-esterified into phospholipids and become targets for cPLA$_2$α activity. In agreement with this, TAG synthesis and lipolysis determine phospholipid composition and consequently affect cPLA$_2$α mobilisation of PUFAs for the production of eicosanoids.

Lipid droplets drive cancer cell proliferation by promoting eicosanoid production

Prostaglandin E$_2$ and other eicosanoids are mitogenic factors that promote cancer cell proliferation (Wang & DuBois, 2010). Based on our findings showing that lipid droplets are required for lipid mediator production, we next examined whether lipid droplets and their breakdown via ATGL-mediated lipolysis promote the proliferation of cancer cells. As hGX

sPLA$_2$ stimulates the proliferation of MDA-MB-231 and other cancer cells (Surrel *et al*, 2009; Pucer *et al*, 2013), we first investigated whether lipid droplet depletion by inhibition of DGAT-mediated TAG synthesis blocks this proliferative effect. Here, the induction of cell proliferation by hGX sPLA$_2$ was fully blocked by DGAT1 inhibition and by concurrent inhibition of both DGAT1 and DGAT2; however, DGAT2 inhibition alone had no effects (Fig. 8A). Importantly, inhibition of DGAT1, but not DGAT2, also reduced the basal, hGX-sPLA$_2$-independent rate of breast cancer cell proliferation. As ATGL overexpression promotes PGE$_2$ production, we hypothesized that ATGL overexpression should induce cell proliferation in a COX/LOX-dependent manner. Indeed, alone or in combination with sPLA$_2$ treatments, ATGL overexpression stimulated the proliferation of breast cancer cells (Fig. 8B, C). Importantly, both hGX-sPLA$_2$-mediated and ATGL-mediated cell proliferation were suppressed by indomethacin and nordihydroguaiaretic acid, which are non-selective COX and LOX inhibitors, respectively (Fig. 8B, C). This suggested that the conversion of hGX-sPLA$_2$-released and ATGL-released PUFAs into lipid mediators is responsible for the mitogenic effects. After being secreted into the extracellular space, eicosanoids can act on neighbouring cells by binding to their cognate G-protein-coupled receptors that activate various signalling pathways (Wang & DuBois, 2010; Jarc & Petan, 2020). To confirm the mitogenic potency of PGE$_2$ under the present conditions, cell proliferation was measured in MDA-MB-231 cells treated with exogenous PGE$_2$. As expected, PGE$_2$ stimulated cell proliferation, although, interestingly, this effect was suppressed by inhibition of DGAT1-dependent TAG synthesis (Fig. 8D), but not by DGAT2 inhibition. This suggested a positive-feedback loop between eicosanoids and DGAT1-mediated lipid droplet turnover.

cPLA$_2$α-induced eicosanoid production has already been shown to promote cancer cell proliferation and tumour growth (Leslie, 2015; Koundouros *et al*, 2020), although this activity has not been associated with lipid droplets. As cPLA$_2$α has a major role in lipid droplet-dependent eicosanoid production in A549 cells (Fig. 5B), we asked whether cPLA$_2$α overexpression stimulates A549 cell proliferation in a DGAT-dependent manner. Indeed, DGAT inhibition fully blocked cPLA$_2$α-overexpression-induced cell proliferation (Fig. 8E), which confirmed that DGAT-mediated lipid droplet biogenesis is required for cPLA$_2$α-stimulated A549 lung cancer cell proliferation. This A549 cell proliferation was suppressed by the COX inhibitor indomethacin (Fig. 8E), which suggested that it depends on COX-mediated conversion of cPLA$_2$α-released AA into mitogenic lipid mediators, such as PGE$_2$. Importantly, exogenous hGX sPLA$_2$ also stimulated A549 cell proliferation, which was suppressed by inhibition of DGAT and COX (Fig. 8E). Finally, in MDA-MB-231 cells, where we found that DGAT-mediated TAG synthesis is required for cPLA$_2$α-stimulated PGE$_2$ production (Fig. 5D), cPLA$_2$α overexpression resulted in higher proliferation rates, which were reduced by DGAT inhibition (Fig. 8F).

Together, these data demonstrate that DGAT1-dependent TAG synthesis and lipid droplet formation are involved in hGX-sPLA$_2$-, cPLA$_2$α- and ATGL-mediated, COX- and LOX-dependent eicosanoid production and for cancer cell proliferation.

Discussion

In this study, we provide evidence that lipid droplet turnover is required for the production of a wide range of pro-inflammatory and anti-inflammatory PUFA-derived lipid mediators in cancer cells. We show that the esterification of PUFAs into TAGs and their release from lipid droplets is necessary for their entry into lipid mediator production pathways. Namely, impeding the incorporation of PUFAs, either added exogenously or derived from hGX sPLA$_2$ membrane hydrolysis, into lipid droplets by inhibition of DGAT-mediated TAG synthesis, or blocking PUFA release from TAGs by silencing ATGL, compromises lipid mediator production under starvation conditions. Lipid droplet turnover is also required for stimulation of eicosanoid production by cPLA$_2$α, the canonical PLA$_2$ responsible for AA release from membrane phospholipids. The data from the aggressive breast cancer cells suggest that ATGL-mediated TAG lipolysis promotes the incorporation of PUFAs into phospholipids. cPLA$_2$α acts downstream of lipid droplet breakdown and targets PUFA-rich phospholipids. Furthermore, although ATGL was dispensable for lipid mediator production in the A549 lung cancer cells, uninterrupted TAG synthesis was still necessary for basal and cPLA$_2$α-induced eicosanoid production in these cells. In summary, this study identifies the lipid droplet organelle as a central hub of lipid mediator synthesis pathways underlying cancer cell proliferation.

DGAT-mediated TAG synthesis is required for eicosanoid production in cancer cells

The trafficking of PUFAs between membranes and lipid droplets is emerging as a major mechanism in the control of PUFA oxygenation and in the protection of various cells against oxidative damage (Bailey *et al*, 2015; Jarc *et al*, 2018; Dierge *et al*, 2021). In immune and cancer cells, lipid droplets have been implicated in AA storage and trafficking, and they have also been suggested to act as platforms for eicosanoid production (Dvorak *et al*, 1983; Triggiani *et al*, 1994; Bozza *et al*, 2011). Accordingly, the release of PUFAs from TAGs via ATGL/HSL-mediated lipolysis has been shown to promote eicosanoid production in immune cells and adipocytes (Dichlberger *et al*, 2014; Schlager *et al*, 2015; Gartung *et al*, 2016).

Here, we show that DGAT-mediated incorporation of PUFAs into TAGs stored within lipid droplets, and their subsequent release via lipolysis, are indeed required for eicosanoid production, which, in turn, drives cancer cell proliferation. In agreement with this, it was shown

recently that DGAT1-mediated TAG synthesis is required for PGE_2 production and activation of inflammatory macrophages (Castoldi *et al*, 2020). Moreover, a recent study showed that lipid droplet biogenesis by DGAT1 is necessary for prostaglandin synthesis during *Drosophila* oogenesis (preprint: Giedt *et al*, 2021). One of the most striking findings of the present study is that DGAT controls eicosanoid production and cancer cell proliferation suggesting that the build-up of PUFA-rich TAG stores drives eicosanoid production pathways. A similar mechanism has been described in cardiomyocytes, whereby exogenous FAs have to be esterified into TAGs and then released by ATGL to activate peroxisome-proliferator-activated receptor (PPAR) signalling pathways (Haemmerle *et al*, 2011; Zechner *et al*, 2012). Furthermore, as DGAT activity is a prerequisite for both ATGL-induced and $cPLA_2\alpha$-induced eicosanoid production in serum-starved cancer cells, it can be assumed that lipid droplets control PUFA availability for eicosanoid production through regulation of both the TAG and membrane phospholipid pools.

Based on our results that suggest that lipid droplets drive lipid mediator production and cancer cell proliferation via the control of PUFA trafficking through the TAG and phospholipid pools, we propose that targeting the DGAT enzymes might improve cancer treatments, particularly under conditions of elevated lipid influx (e.g., abundance of dietary fats, oncogene-driven elevated endogenous FA synthesis, high autophagic flux). Indeed, DGAT1 was identified recently as a potent oncoprotein that increases the resilience of cancer cells against the stress of increased FA acquisition, which is a hallmark of transformed cells (preprint: Wilcock *et al*, 2020). Furthermore, our previous data showed that breast cancer cells challenged with exogenous PUFAs depend on the balance between DGAT1-mediated sequestration of PUFAs into lipid droplets and their release via ATGL-mediated lipolysis to survive lethal oxidative damage (Jarc *et al*, 2018). In support of this, inhibition of DGAT activity diverts dietary PUFAs towards esterification into membrane phospholipids, thereby increasing their peroxidation and leading to ferroptosis in acidic tumours (Dierge *et al*, 2021). Interestingly, high levels of dietary AA in mice compromise $cPLA_2\alpha$ inhibitor-mediated suppression of eicosanoid production and *PIK3CA* mutant-driven tumour growth (Koundouros *et al*, 2020). Although the involvement of lipid droplet metabolism was not assessed in this study, it will be important to examine whether lipid droplets control the supply of AA for eicosanoid production under this and similar scenarios.

Our results suggest that DGAT activity controls cancer cell proliferation by generating PUFA stores in lipid droplets, which can be used for the production of potent, albeit short-lived, pro-inflammatory and anti-inflammatory lipid signalling molecules. As these signalling molecules are released from cells to act in autocrine and paracrine manners, they can modulate tumour growth by altering the function of cancer cells, immune cells and other cells in the tumour microenvironment (Wang & DuBois, 2010; Greene *et al*, 2011). Thus, in addition

to their protective role against nutrient deficiency, lipotoxicity and oxidative stress in cancer cells (Petan, 2020), lipid droplets modulate tumour growth through the control of lipid mediator-dependent cell-autonomous and non-cell-autonomous mitogenic and inflammatory signalling pathways, and are thus a promising target for therapeutic intervention.

Lipid droplets control hGX-sPLA$_2$-induced and cPLA$_2$α-induced eicosanoid production

Several members of the sPLA$_2$ family are involved in lipid mediator production under various inflammatory conditions, including cancers (Brglez *et al*, 2014a). Group X sPLA$_2$ is the most potent enzyme among mammalian sPLA$_2$s in terms of its binding to and hydrolysis of the phosphatidylcholine-rich extracellular leaflet of mammalian cells, thereby releasing various unsaturated FAs and PUFAs, and stimulating lipid mediator production (Hanasaki *et al*, 1999; Bezzine *et al*, 2002; Surrel *et al*, 2009; Murase *et al*, 2016; Jarc *et al*, 2018). Some other sPLA$_2$ isoforms, such as group IIA sPLA$_2$s, bind very poorly to phosphatidylcholine-rich membranes, and thus do not hydrolyse the plasma membranes of resting cells, but instead depend on their internalisation and interaction with intracellular cPLA$_2$α to promote eicosanoid production (Lambeau & Gelb, 2008). Here, we show that both hGX sPLA$_2$ and cPLA$_2$α depend on lipid droplet turnover to drive lipid mediator production in cancer cells.

Our finding that PUFAs released by hGX sPLA$_2$ from cancer cell membranes and serum lipoproteins are incorporated into growing lipid droplets, thereby enriching TAGs with various ω-3 and ω-6 PUFAs, is important because it identifies a mechanism of enzymatically induced enrichment of lipid droplets with phospholipid-derived PUFAs. Its relevance is not likely to be limited to *in vitro* conditions, because group X sPLA$_2$ has been shown to modulate lipid metabolism and adipogenesis *in vivo* (Li *et al*, 2010; Shridas *et al*, 2010; Sato *et al*, 2011), to promote release of ω-3 and ω-6 PUFAs and their conversion into lipid mediators in several tissues (Murase *et al*, 2016; Murakami *et al*, 2020), and to control intestinal lipid mediator production, inflammation and tumorigenesis *in vivo* (Schewe *et al*, 2016). Furthermore, PUFA-enriched TAGs have been observed in visceral adipose tissue of patients with colorectal cancer, along with elevated expression of hGX sPLA$_2$ and prostaglandin-biosynthetic enzymes (Liesenfeld *et al*, 2015).

Although the sPLA$_2$-treated MDA-MB-231 breast cancer cells showed an enrichment of both TAGs and phospholipids with PUFAs, their release from TAGs by ATGL was essential for their conversion into lipid mediators. On the contrary, in the A549 lung cancer cells, ATGL was not necessary for lipid mediator production and the silencing of cPLA$_2$α suppressed hGX-sPLA$_2$-induced PGE$_2$ production. Even in these cells, however, we showed that intact TAG synthesis is a prerequisite for both hGX-sPLA$_2$-induced and cPLA$_2$α-induced eicosanoid synthesis and cancer cell proliferation. These results are important because the provision of PUFAs for conversion into lipid mediators by two of the most potent mammalian PLA$_2$s has

been shown here to depend on lipid droplet turnover. Our results thus provide a novel view of PLA_2-mediated inflammatory signalling, which tightly integrates PLA_2-mediated regulation of PUFA availability with cellular lipid droplet metabolism. Lipid droplets could be the missing link that will help explain the elusive cross-talk between $sPLA_2$s and $cPLA_2\alpha$ in lipid mediator biosynthesis (Mounier *et al*, 2004; Saiga *et al*, 2005; Lambeau and Gelb, 2008). We speculate that the relevance of these findings extends beyond cancer cells to various pathophysiological settings, whereby context-specific characteristics of FA and lipid droplet metabolism will modulate, or even govern, PLA_2-induced inflammatory lipid mediator production.

Our results indicate that different cell-type-specific mechanisms might explain the dependence of $cPLA_2\alpha$-induced eicosanoid production on lipid droplets. In the MDA-MB-231 and HeLa cells, $cPLA_2\alpha$ depended on TAG synthesis and ATGL-mediated TAG lipolysis to drive the incorporation of AA (and other PUFAs) into phospholipids, which were then targeted by $cPLA_2\alpha$. In A549 cells, $cPLA_2\alpha$ controls basal and $sPLA_2$-induced PGE_2 production independently of ATGL, although its activity still depends on TAG synthesis. In both cases, our data suggest that $cPLA_2\alpha$-mediated AA release for eicosanoid production occurs downstream of, and is controlled by, lipid droplet turnover. Interestingly, $cPLA_2\alpha$ has also been shown to drive mitochondrial β-oxidation of both FAs and eicosanoids for energy production (Slatter *et al*, 2016), which is another indication that ATGL and $cPLA_2\alpha$ share common metabolic and signalling pathways. Altogether, our findings suggest that lipid droplet turnover regulates the supply of PUFAs for the lipid mediator production machinery via at least two pathways: direct $cPLA_2\alpha$-independent delivery of TAG lipolysis-derived PUFAs via ATGL; and an indirect $cPLA_2\alpha$-dependent route that involves lipolysis-induced phospholipid acyl-chain remodelling that controls the availability of PUFAs for (c)PLA_2-induced lipid mediator production. Notably, our data indicate that other lipases and lipid droplet breakdown mechanisms (e.g., lipophagy) besides (or instead of) ATGL might contribute to lipid droplet-dependent lipid mediator biosynthesis.

One of the intriguing questions that remains to be addressed in future studies is whether PUFA trafficking between the TAG core and the lipid droplet phospholipid monolayer is relevant for lipid mediator production. In principle, TAG lipolysis-derived PUFAs can be re-esterified in monolayer phospholipids and targeted by $cPLA_2\alpha$ or other PLA_2s. In agreement with this, $cPLA_2\alpha$, COXs, several prostaglandin synthetases and *de-novo* produced eicosanoids have been localised to lipid droplets (Wooten *et al*, 2008; Moreira *et al*, 2009; Bozza *et al*, 2011; Cruz *et al*, 2020; Ward *et al*, 2020). The molecular basis and functional relevance of these findings is currently unclear, but we speculate that eicosanoid production does not necessarily occur on lipid droplets as isolated cytosolic platforms, but at specific lipid droplet–ER contact sites that provide rapid lipid and protein transfer between the lipid structures involved (i.e., the ER membrane bilayer, the lipid droplet phospholipid monolayer

and TAG core) (Schuldiner & Bohnert, 2017). Such compartmentalisation would support the interplay among cPLA$_2$α, ATGL and other enzymes in the control of lipid droplet turnover, membrane remodelling and the eicosanoid synthesis machinery.

cPLA$_2$α modulates membrane PUFA-phospholipid content and lipid droplet metabolism

Our results also indicate that cPLA$_2$α-induced membrane remodelling affects lipid droplet dynamics. We showed that cPLA$_2$α silencing induces significant changes in lipid droplet numbers, neutral lipid content, and phospholipid and TAG acyl-chain compositions. Previous studies have shown that cPLA$_2$α is involved in remodelling of membrane shape, and that it might facilitate lipid droplet biogenesis in severely-starved cells (Gubern *et al*, 2008; Guijas *et al*, 2014; Astudillo *et al*, 2019; Jarc & Petan, 2020). Intriguingly, the N-terminal membrane-binding C2 domain of cPLA$_2$α is sufficient to induce changes in membrane shape, and it selectively localises to lipid droplets (Ward *et al*, 2012, 2020). However, our findings that cPLA$_2$α depletion leads to elevated TAG accumulation and increases lipid droplet numbers during serum starvation argue against a mechanism in which cPLA$_2$α promotes lipid droplet biogenesis. On the contrary, the increased numbers of lipid droplets upon cPLA$_2$α silencing (particularly in serum-starved cells when TAG lipolysis is activated) might instead reflect secondary activation of lipid droplet biogenesis, which can occur under lipolytic conditions to sequester excess free FAs and to reduce lipotoxicity (Paar *et al*, 2012; Chitraju *et al*, 2017; Schott *et al*, 2019).

In line with this idea, our lipidomic data suggest that the changes in TAG acyl-chain composition as a result of cPLA$_2$α depletion are dependent on ATGL. Furthermore, our lipid ontology enrichment analysis suggests that the elevated PUFA content in membrane phospholipids of cPLA$_2$α-depleted cells is indicative of changes in membrane biophysical properties, including fluidity, thickness and bending properties (Antonny *et al*, 2015), which might facilitate lipid droplet biogenesis. Indeed, PUFA-containing phospholipids have recently been shown to induce seipin enrichment at specific ER–lipid droplet contact sites, to thereby promote the expansion of nascent lipid droplets (Cao *et al*, 2019). Furthermore, elevated acyl-chain unsaturation and phosphatidylethanolamine content in ER membranes, along with a reduction in overall TAG saturation, have been shown to strongly promote lipid droplet nucleation (Zoni *et al*, 2021). We thus propose that cPLA$_2$α modulates membrane PUFA composition in serum-starved cancer cells, to thereby fine-tune its biophysical properties, which indirectly affects lipid droplet biogenesis (and possibly also lipolysis at the lipid droplet phospholipid monolayer). Depletion of cPLA$_2$α in serum-starved cancer cells induces a gradual enrichment of PUFAs in phospholipids that might in turn alter the membrane properties in a way that favours lipid droplet biogenesis. It remains to be established in future studies whether

these hypotheses can explain the relationships between cPLA$_2$α, lipid droplet turnover and lipid droplet-dependent lipid mediator production.

In conclusion, our study reveals that lipid droplets are essential for lipid mediator production and cancer cell proliferation. Esterification of PUFAs into TAGs by the DGAT enzymes and PUFA release from lipid droplets (which depends on TAG lipolysis by ATGL, and/or other lipases in some cancer cells) drives lipid mediator production either directly, by feeding PUFAs into the COX/LOX machinery, or by redirecting some of the PUFAs into membrane phospholipids first, whereby they are then targeted by cPLA$_2$α. Notably, both exogenous and sPLA$_2$-membrane-hydrolysis-derived PUFAs have to cycle through lipid droplets to be converted into lipid mediators, which reveals that lipid droplets are not optional storage reservoirs for excess PUFAs, but instead consolidate different PUFA sources and actively control PUFA release. Lipid droplets thus have an important regulatory role in lipid mediator production, thereby potentially affecting numerous downstream signalling pathways that are involved in inflammation, immunity and cancer.

Materials and methods

Materials

MDA-MB-231 human breast adenocarcinoma cells, A549 human lung carcinoma cells, HeLa human cervical adenocarcinoma cells, C2C12 mouse myoblasts cells, and Caco-2 human colorectal adenocarcinoma cells were obtained from American Type Culture Collection (ATCC, USA). J774A.1 mouse reticulum cell sarcoma macrophages were from the European Collection of Authenticated Cell Cultures (ECACC, UK), and MDA-MB-231 human breast adenocarcinoma cells with stable luciferase 2A and RFP expression (MDA-MB-231/Luciferase-2A-RFP) were from GeneTarget (USA). PC-3 human prostate adenocarcinoma cells were a kind gift from Dr. Mojca Pavlin (University of Ljubljana, Slovenia). OV-90 human ovarian papillary serous adenocarcinoma cells, TOV-112D human ovarian endometrioid carcinoma cells, TOV-21G human ovarian clear cell carcinoma cells and Ishikawa human endometrial adenocarcinoma cells were a kind gift from Dr. Brett McKinnon (Berne University Hospital, Switzerland). SGBS human Simpson-Golabi-Behmel syndrome preadipocytes were a kind gift from Dr. Merce Miranda (Joan XXIII University Hospital Tarragona, Spain), and SH-SY5Y human neuroblastoma cells were a kind gift from Dr. Boris Rogelj (Jožef Stefan Institute, Slovenia). RPMI-1640 culture medium was from ATCC (USA), and Dulbecco's modified Eagle's medium nutrient mixture F-12 (DMEM/F12), DMEM with high glucose and GlutaMAX supplement (DMEM-GlutaMax), foetal bovine serum, Dulbecco's

779 phosphate-buffered saline (DPBS), TrypLE Select and Opti-MEM were from Life Technologies
780 (USA). AA and PGE_2 standards were from Cayman Chemical (USA), and BODIPY 493/503,
781 Lipofectamine RNAiMAX, Lipofectamine 3000, High-capacity cDNA reverse transformation
782 kits were from Thermo Fisher Scientific (USA). Hoechst 33342 nuclear stain was from Enzo
783 Life Sciences (USA). Human ATGL-targeting and $cPLA_2\alpha$-targeting siRNAs and the AllStars
784 Negative Control siRNA were from Qiagen (Germany). T863 (DGAT1 inhibitor), PF-06424439
785 (DGAT2 inhibitor), indomethacin (COX inhibitor), nordihydroguaiaretic acid (LOX inhibitor),
786 essentially fatty acid-free (EFAF) bovine serum albumin (BSA) (cat. no. A7511), FAF-BSA (cat.
787 no. A8806) and Nile red were from Sigma-Aldrich (USA). High Pure RNA isolation kits were
788 from Roche (Germany), horseradish-peroxidase-labelled secondary antibodies were from
789 Jackson ImmunoResearch Laboratories (USA), ATGL antibodies (cat. no. #2138) were from
790 Cell Signaling Technology (USA), $cPLA_2\alpha$ antibodies (cat. no. sc-454) were from Santa Cruz
791 (USA) and β-actin antibodies (cat. no. NB600-532) were from Novus Biologicals (UK).
792 Recombinant wild-type hGX $sPLA_2$ was prepared as described previously (Pucer *et al*, 2013).
793 The full-length cDNAs coding for human $cPLA_2\alpha$ (NCBI RefSeq NM.024420.3) and ATGL
794 (NCBI RefSeq NM.020376.4) were cloned into the pcDNA 4/HisMaxC vector (Thermo Fisher
795 Scientific, USA) using Gibson assembly cloning kits (New England Biolabs, USA), after
796 removal of the N-terminal His-tag region. All of the other chemicals were of at least analytical
797 grade, and were purchased from Sigma-Aldrich (USA) or Serva (Germany).
798
799 ***Cell culture and treatments***
800 MDA-MB-231 cells were cultured in RPMI-1640 medium, A549 cells in DMEM/F12 medium
801 containing 2 mM L-glutamine (Gibco, USA), and HeLa cells in DMEM-Glutamax medium, all
802 supplemented with 10% foetal bovine serum. Adherent cells were detached using TrypLE
803 Select. Unless otherwise indicated, the cells were seeded in 24-well plates at a density of 3
804 $\times 10^4$ (MDA-MB-231), 2.5 $\times 10^4$ (A549) or 1.5 $\times 10^4$ (HeLa) cells/well and grown for 48 h in
805 complete medium, followed by 24 h of serum deprivation in their respective media containing
806 0.02% EFAF-BSA. Aliquots of stock solutions of AA and PGE_2 in absolute ethanol were stored
807 under argon at –80 ºC. Prior to addition to cell cultures, AA was resuspended in the relevant
808 complete medium and incubated for 1 h at room temperature. Unless otherwise indicated,
809 T863 and PF-06424439 were added to cells 2 h before treatments with recombinant hGX
810 $sPLA_2$ (1–10 nM) or AA (10 μM), and were present in the medium for the duration of the
811 treatments. Prior to addition to cell culture, radiolabelled [^{14}C]-OA was saponified by removing
812 ethanol from the stock aliquot of [^{14}C]-OA and resuspending in 50 μL 0.1 mM NaOH. Saponified
813 [^{14}C]-OA was incubated in the relevant complete medium for 30 min at room temperature and
814 stored at –20 ºC.
815

816 ***Silencing of ATGL and cPLA$_2$α expression using small-interfering RNAs***

817 Reverse transfection was performed in 24-well plates at cell densities of 6 ×10^4 (MDA-MB-
818 231), 5 ×10^4 (A549) or 3 ×10^4 (HeLa) cells/well, or in 6-well plates at 3 ×10^5 (MDA-MB-231),
819 2.5 ×10^5 (A549) or 1.5 ×10^5 (HeLa) cells/well. Gene expression silencing was performed with
820 a 20 nM mixture of two ATGL-specific siRNAs (10 nM each) or a 40 nM mixture of four siRNAs
821 specific for cPLA$_2$α. Non-targeting siRNA controls contained 20 nM (for ATGL) or 40 nM (for
822 cPLA$_2$α) AllStars Negative Control siRNA (Qiagen). Transfection complexes were generated
823 using 1 µL/well Lipofectamine RNAiMAX in 24-well plates, or 7.5 µL/well in 6-well plates, with
824 Opti-MEM medium, according to manufacturer instructions.
825
826 ***Transient overexpression of ATGL and cPLA$_2$α***
827 For transient overexpression experiments, the cells were seeded in complete medium in 24-
828 well plates at a density of 9 ×10^4 (MDA-MB-231), 6 ×10^4 (A549) and 4.5 ×10^4 (HeLa) cells/well,
829 or in 6-well plates at 4.5 ×10^5 (MDA-MB-231), 3 ×10^5 (A549) and 2.5 ×10^5 (HeLa) cells/well.
830 Cells were then incubated for 24 h in complete medium, washed, and transfected with 0.5
831 µg/well plasmid DNA in 24-well plates, or 2.5 µg/well in 6-well plates, using Lipofectamine 3000
832 and Opti-MEM medium, according to manufacturer instructions; they were then left for 6 h in
833 serum-depleted medium containing 0.02% EFAF-BSA (serum starvation). After 6 h, the cells
834 were washed and treated according to the experimental set-up.
835
836 ***Real-time quantitative PCR***
837 Real-time quantitative (q)PCR analysis was performed as described previously (Pucer *et al*,
838 2013; Brglez *et al*, 2014b). Briefly, the cells were seeded in complete medium in 6-well plates
839 at 3 ×10^5 (MDA-MB-231), 2.5 ×10^5 (A549) and 1.5 ×10^5 (HeLa cells) cells/well, grown 48 h in
840 complete medium, followed by 24 h under serum deprivation in medium containing 0.02%
841 EFAF-BSA. Total RNA was isolated from cell lysates and first-strand cDNA was generated
842 using High-Capacity cDNA Reverse Transcription kits (Applied Biosystems, USA), according
843 to the manufacturer instructions. qPCR analysis was performed on a StepOnePlus real-time
844 PCR system (Thermo Scientific, USA) using FastStart Universal SYBR Green Master (Rox;
845 Roche, Switzerland). Calibrator cDNA was transcribed from Quantitative PCR Human
846 Reference Total RNA (Agilent Technologies, USA). Relative gene expression was calculated
847 upon normalisation to two reference genes, considering primer-specific PCR efficiency and
848 error propagation.
849

Western blotting

The cells were seeded in complete medium in 6-well plates and reverse transfected with siRNAs and/or transiently transfected with pDNA, as described above. Cell lysates were prepared by scrapping adherent cells in Tris-glycine sodium dodecyl sulphate (SDS) sample buffer (2×) (Novex, Life Technologies, USA) that contained 800 mM dithiothreitol (Sigma-Aldrich, USA), with the addition of Halt protease inhibitor cocktail (Thermo Scientific, USA). Lysates were incubated at 95 °C for 10 min and stored on ice. Total protein concentrations were determined using Pierce 660 nm protein assays (Thermo Scientific, USA). Proteins (10–40 µg) were separated on 10% SDS-PAGE gels and then transferred to nitrocellulose membranes (Serva, Germany). The membranes were blocked for 1 h (for ATGL) or 2 h (for cPLA$_2$α) in 5% non-fat dry milk in TBS/0.1% Tween-20 (TBST) or in 1% Western blocking reagent (WBR) (Roche Applied Science, Germany) in TBS (for β-actin), and incubated overnight at 4 °C in the presence of rabbit anti-human primary antibodies for ATGL (1:1000 dilution) or mouse anti-human primary antibodies for cPLA$_2$α (1:250 dilution), both in 5% non-fat dry milk in TBST, or in rabbit anti-human primary antibodies for β-actin (1:5000 dilution) in 0.5% WBR in TBS. After washing with TBST, the membranes were incubated for 1 h with horseradish-peroxidase-conjugated secondary antibodies (1:10,000 dilution) in 5% non-fat dry milk in TBST for ATGL, in 0.5% WBR in TBST for cPLA$_2$α, and in 0.5% WBR in TBS for β-actin. The signals were visualised using Lumi-Light Western Blotting Substrate (Roche Applied Science, Germany) on a Gel Doc XR system (Bio-Rad, USA).

Neutral lipid quantification by flow cytometry

Cellular neutral lipid levels were quantified by flow cytometry as described previously (Pucer *et al*, 2013). Floating and adherent cells were harvested and centrifuged at 300× *g* for 10 min, and the pellets were resuspended in 500 µL 1 µg/mL Nile Red solution in DPBS. After a 10-min incubation in the dark, cell analysis was performed by flow cytometry on a FACSCalibur system, equipped with a 488-nm Ar-ion laser, and using the CellQuest software (Becton Dickinson, USA) and an FL-1 (530/30) filter, for at least 2 ×10^4 events per sample.

Triglyceride assays

Cellular TAG contents were determined using TAG assay kits - quantification (Abcam, USA). MDA-MB-231 and HeLa cells were seeded in 6-well plates at 1.5 ×10^5 and 7 ×10^4 cells/well, respectively. After 24 h, MDA-MB-231 cells were treated with 10 nM hGX sPLA$_2$ and HeLa cells with 1 nM hGX sPLA$_2$ in complete medium for 48 h. Cell lysates were prepared and used for TAG quantification according to the manufacturer instructions.

Glycerol release assays

Cellular lipolytic activity was assessed by measuring glycerol release in cell supernatants. Briefly, the cells were reverse transfected and seeded in 48-well plates at a density of 3 ×10^4 (MDA-MB-231 cells) or 1.5 ×10^4 cells/well (HeLa cells). For reverse transfection, 0.5 µL Lipofectamine RNAiMAX, 20 nM siRNA and 40 µL OPTI-MEM medium were used per well. After 24 h, the cells were washed, placed in serum-starvation medium containing 0.02% EFAF-BSA, and transfected with 0.250 µg plasmid DNA for protein overexpression using Lipofectamine 3000, according to the manufacturer instructions. After 6 h, the cells were washed and treated with 10 nM hGX $sPLA_2$ for 48 h in complete medium. Cell supernatants were collected in low-binding microcentrifuge tubes and centrifuged for 10 min (4 °C, 16,000× *g*), and the glycerol concentrations were determined using the Glycerol Cell-Based assay kits (Cayman Chemicals, USA), according to the manufacturer instructions.

Untargeted lipidomic analysis of phospholipids and triglycerides

For untargeted lipidomic analysis of hGX-$sPLA_2$-induced changes in TAG acyl-chain composition, MDA-MB-231 cells were seeded in complete medium on 10-cm plates at 1 ×10^6 cells/plate. After 24 h, the cells were treated with 1 nM hGX $sPLA_2$ in complete medium for 48 h. Cell lysates were prepared by washing the cells twice with DPBS and scraping in 1 mL lysis buffer (20 mM Tris-HCl, pH 7.4, 2 mM EDTA, 2 µL Halt protease inhibitor cocktail), followed by centrifugation for 10 min (1000× *g*, 4 °C). Cell pellets were resuspended in 150 µL lysis buffer and sonicated on ice. Total lipids were extracted in chloroform/methanol (2/1, v/v) containing 1% acetic acid, 500 nM butylated hydroxytoluene (BHT) and internal standards (IS; 100 pmol 17:0/17:0/17:0 triacylglycerol, Larodan, Solna, Sweden) under constant shaking for 1 h (30 rpm/min, 4 °C). After centrifugation at 3300 rpm for 20 min at room temperature, the upper aqueous layer was removed, and the organic solvents were evaporated using a sample concentrator (Techne, UK) equipped with the Dri-Block DB-3 heater (Techne, UK). Lipids were resolved in 200 µL chloroform and stored at –20 ºC. Prior to mass spectrometry, the samples were placed at room temperature and dried and resuspended in 1 mL chloroform/methanol (2/1, v/v). An aliquot of each sample (20 µL) was mixed with 180 µL isopropanol, and 5 µL was used for chromatographic separation on an Acquity-UPLC system (Waters Corporation, Milford, MA, USA), equipped with an ACQUITY BEH C18 column (2.1 × 50 mm, 1.7 µm; Waters Corporation, Milford, MA, USA). A SYNAPT^{TM}G1 qTOF HD mass spectrometer (Waters Corporation, Milford, MA, USA) equipped with an ESI source was used for detection. Data acquisition was carried out using the MassLynx 4.1 software (Waters), and the lipid classes were analysed with the Lipid Data Analyser 1.6.2 software. The data were normalised for recovery, extraction and ionisation efficacy by calculating analyte/internal standard ratios (AU) and expressed as percentage composition.

To determine the changes in the phospholipid and TAG profiles in ATGL-depleted and cPLA$_2$α-depleted cells, MDA-MB-231 cells were seeded in complete medium on 6-well plates at 3 ×10^5 cells/well and reverse transfected with ATGL-specific and/or cPLA$_2$α-specific siRNAs, as described above. After 24 h, the cells were washed and grown for 48 h in complete medium in the presence or absence of 10 nM sPLA$_2$. The cells were then washed twice with DPBS and serum starved for the following 24 h in RPMI-1640 medium containing 0.02% EFAF-BSA. Samples were collected (at 0, 3, 24 h of serum starvation) by placing the plates on ice, washing the cells twice with ice-cold DPBS, and scraping the cells in 300 µL lysis buffer, followed by centrifugation for 10 min (1000× *g*, 4 °C). The cell pellets were resuspended in 150 µL lysis buffer and sonicated on ice. Then, 10 µL of each sample was used for protein determination (Pierce 660). Total lipids were extracted by transferring the pellets into 2 ml tubes followed by homogenisation in 700 µL of a 3:1 (v/v) mixture of methyl tert-butyl ether and methanol, containing 1% acetic acid, 500 nM BHT and IS (8 pmol 18:3/18:3/18:3 triacylglycerol, 14:0/14:0 phosphatidylcholine, Larodan, Solna, Sweden; 50 pmol 17:0/17:0 phosphatidylethanolamine, 12 pmol 17:0/17:0 phosphatidylserine, Avanti Polar Lipids, Alabaster, AL, USA), with two steel beads on a mixer mill (30 Hz, Retsch, Germany) at 4 °C. After homogenisation, the samples were mixed at room temperature under constant shaking for 30 min. Then 140 µL distilled H_2O was added, and the samples were thoroughly mixed and centrifugated (14,000 rpm, 10 min), to establish phase separation. The organic phase (500 µL) was transferred into new tubes and the organic solvent was evaporated off under a stream of nitrogen. The residual protein slurry was dried and used for protein determination after lysis in 400 µL NaOH/SDS (0.3 M/0.1%). Prior to mass spectrometry analysis, the lipids were resolved in 200 µL isopropanol /methanol/H_2O (70/25/10, v/v/v). Chromatographic separation was performed on a 1290 Infinity II LC system (Agilent, Santa Clara, CA, USA) equipped with a C18 column (Zorbax RRHD Extend; 2.1 × 50 mm, 1.8 µm; Agilent, Santa Clara, CA, USA), using a 16 min linear gradient from 60% solvent A (H_2O; 10 mM ammonium acetate, 0.1% formic acid, 8 µM phosphoric acid) to 100% solvent B (2-propanol; 10 mM ammonium acetate, 0.1% formic acid, 8 µM phosphoric acid). The column compartment was kept at 50 °C. A Q-TOF mass spectrometer (6560 Ion Mobility; Agilent, Santa Clara, CA, USA) equipped with electrospray ionisation source (Dual AJS) was used for detection of the lipids in positive and negative Q-TOF mode. Data acquisition was carried out using the MassHunter Data Acquisition software (B.09; Agilent, Santa Clara, CA, USA). Lipid species were manually identified and lipid data were processed using MassHunter Quantitative Analysis (B.09.00; Agilent, Santa Clara, CA, USA). Data were normalised for recovery, extraction and ionisation efficiency by calculation of the analyte/ internal standard ratios, and are expressed as fmol/µg protein. Lipidomic data were analysed by multiple t-test analysis of log-transformed data to compare two conditions at a time, using GraphPad Prism 9.0.2 (GraphPad Software, USA). Lipid ontology enrichment

analysis was performed using the LION/web enrichment and principal component analysis modules (Molenaar *et al*, 2019).

Thin layer chromatography of radiolabelled cellular lipids

MDA-MB-231 cells were seeded in complete medium on T-25 flasks at a density of 5 ×10^5 cells/flask. After 24 h, the cells were treated with 1 µCi/sample [^{14}C]-OA for 18 h, washed twice with DPBS, and treated with 10 nM hGX sPLA$_2$ under three different conditions: (a) 24 h in complete medium; (b) 24 h in complete medium followed by 96 h serum deprivation in 0.02% EFAF-BSA in RPMI-1640; and (c) 24 h in 0.02% FAF-BSA in RPMI-1640 followed by 96 h in 0.02% EFAF-BSA in RPMI-1640. Lipid extraction was performed with 1 mL hexane/ isopropanol (3:2, v/v) under constant shaking for 10 min at room temperature, and repeated twice. The samples were stored in microcentrifuge tubes at –20 ºC. Total proteins were isolated from cell remnants in 2 mL lysis buffer (0.3 M NaOH, 0.1% SDS) under constant shaking for 2 h at room temperature. Protein concentrations were determined using BSA standard solutions (Thermo Scientific, USA) and the BCA protein assay reagent (Thermo Scientific, USA). Samples of cellular lipids were dried, resuspended in 20 µL chloroform (repeated three times), and loaded onto the stationary phase of silica TLC plates immobilised on a polymeric binder (Merck, Germany). Dry TLC plates were developed using chloroform/ methanol/ acetone/ acetic acid/ H_2O (50/10/20/12/5, v/v/v/v/v) for phospholipid separation, and hexane/ diethyl ether/ acetic acid (70:29:1, v/v/v) for neutral lipid separation. Radiolabelled lipids were detected with autoradiography using an imager (PhosphorImager SI; Amersham Biosciences, UK). To quantify the TAG content, the TLC plates were incubated in an iodine steam, the TAG patches were cut out and placed in vials with scintillation cocktail, and the radioactivity was measured using a liquid scintillation counter (Tri-Carb 1600CA; PerkinElmer, USA).

Lipid mediator analysis using UPLC-MS-MS

MDA-MB-231 cells were seeded in complete medium in 6-well plates at 3 × 10^5 cells/well and reverse transfected with ATGL-specific siRNAs as described above. After 24 h, the cells were treated with 10 nM hGX sPLA$_2$ for 48 h, washed with DPBS and left for 24 h in RPMI-1640 medium containing 0.02% EFAF-BSA. The cells were lysed and total protein concentrations were determined as described above. Supernatants were collected in low-binding microcentrifuge tubes, centrifuged at 4 °C (16,000× *g*, 10 min) and stored at –80 °C before shipping on dry ice. Lipid mediator analysis using UPLC-MS-MS was performed as described previously (Werz *et al*, 2018) with some minor modifications (Werner *et al*, 2019). Briefly, aliquots of the supernatants were first mixed with the same volume of ice-cold methanol containing deuterium-labelled internal standards (200 nM d8-5S-HETE, d4-LTB$_4$, d5-LXA$_4$, d5-RvD2, d4-PGE$_2$ and 10 µM d8-AA; Cayman Chemical/Biomol GmbH, Hamburg, Germany) to

facilitate quantification and sample recovery. Samples were kept at −20 °C for 60 min to allow protein precipitation. After centrifugation (1200× *g*, 4 °C, 10 min) 8 mL of acidified H_2O was added (final pH = 3.5) and the samples were subjected to solid phase extraction. The solid phase cartridges (Sep-Pak® Vac 6cc 500 mg/ 6 mL C18; Waters, Milford, MA) were equilibrated with 6 mL methanol and then with 2 mL H_2O prior sample loading onto the columns. After washing with 6 mL H_2O and additional 6 mL *n*-hexane, lipid mediators were eluted with 6 mL methyl formate. The eluates were brought to dryness using a TurboVap LV evaporation system (Biotage, Uppsala, Sweden) and resuspended in 100 µL methanol/water (50/50, v/v) for UPLC-MS-MS analysis. Lipid mediator profiling was analyzed with an Acquity™ UPLC system (Waters, Milford, MA, USA) and a QTRAP 5500 Mass Spectrometer (ABSciex, Darmstadt, Germany), equipped with a Turbo V™ Source and electrospray ionization. Lipid mediators were separated using an ACQUITY UPLC® BEH C18 column (1.7 µm, 2.1 × 100 mm; Waters, Eschborn, Germany) at 50 °C with a flow rate of 0.3 ml/min and a mobile phase consisting of methanol/water/acetic acid of 42/58/0.01 (v/v/v) that was ramped to 86/14/0.01 (v/v/v) over 12.5 min and then to 98/2/0.01 (v/v/v) for 3 min (Werner *et al*, 2019). The QTrap 5500 was operated in negative ionization mode using scheduled multiple reaction monitoring (MRM) coupled with information-dependent acquisition. The scheduled MRM window was 60 sec, optimized lipid mediator parameters were adopted (Werner *et al*, 2019), and the curtain gas pressure was set to 35 psi. The retention time and at least six diagnostic ions for each lipid mediator were confirmed by means of external standards (Cayman Chemical/Biomol GmbH, Hamburg, Germany). Quantification was achieved by calibration curves for each lipid mediator. Linear calibration curves were obtained for each lipid mediator and gave r^2 values of 0.998 or higher (for fatty acids 0.95 or higher). Additionally, the limit of detection for each targeted lipid mediator was determined (Werner *et al*, 2019).

ELISA-based quantification of PGE_2 in cell supernatants

The amounts of PGE_2 released into culture medium were determined using a commercial enzyme immunoassay (Prostaglandin E_2 Express ELISA kits; Cayman Chemicals, USA). The cells were seeded in 24-well plates and reverse transfected with siRNAs as described above. After 24 h, the cells were transfected with plasmid DNA as described above and treated with 10 nM hGX $sPLA_2$ and/or 10 µM AA and/or a mixture of 20 µM T863 and 20 µM PF-06424439 (DGAT inhibitors) for 48 h in complete medium. The cells were then washed and serum starved for 24 h in the appropriate culture medium containing 0.02% EFAF-BSA. In some experiments, DGAT inhibitors were included in the serum-starvation phase. Cell supernatants were collected in low-binding microcentrifuge tubes, centrifuged at 4 °C (16,000× *g*, 10 min) and immediately used for analysis or stored at –80 °C for up to 7 days. For analysis, 50 µL undiluted samples were used, and standard curves prepared by diluting the PGE_2 standard in culture medium.

Confocal microscopy

Cytosolic lipid droplets were visualised using BODIPY 493/503 neutral lipid staining. Cells were reverse transfected and seeded on glass-bottomed culture plates at 6 ×10^4 (MDA-MB-231 cells), 3 ×10^4 (HeLa cells) and 5 ×10^4 (A549 cells) cells/well. Twenty-four hours later, the media were replaced and the cells were treated with 10 nM hGX sPLA$_2$ and the DGAT inhibitors in complete medium for 48 h, followed by 24-h starvation in serum-free medium containing 0.02% EFAF-BSA. For confocal microscopy, the cells were washed twice with DPBS, stained with 1 µg/mL BODIPY 493/503 and 1 µg/mL Hoechst stain solution in RPMI-1640 medium for 15 min in a CO_2 incubator, washed twice with DPBS, and left in fresh RPMI-1640 medium. Live imaging was carried out at the beginning of and after the 24-h serum starvation using a confocal laser scanning microscope (LSM 710; Carl Zeiss, Germany) and a stage-top microscope CO_2 incubation system (Tokai Hit, Japan). Images were processed using the Zen software (Carl Zeiss, Germany).

Lipid droplet counting and diameter analysis

Confocal microscopy images of BODIPY 493/503 stained lipid droplets were used for computer image analysis with the ImageJ software (National Institutes of Health, USA) and the Lipid Droplet Counter Plugin (https://doi.org/10.5281/zenodo.2581434). Analysis was performed on 32-bit two-dimensional images, whereby the numbers and sizes of the lipid droplets were determined according to the plugin instructions. Lipid droplet diameters were calculated from the lipid droplet surface areas. Analyses were performed on at least 40 cells/sample. Data were loaded into the Prism 9.0.2 software (GraphPad Software, USA), with the geometric means of the lipid droplet diameters and numbers calculated per individual cell in the samples, followed by the statistical analysis.

Cell proliferation

MDA-MB-231/Luciferase-2A-RFP cells were seeded in complete medium in 96-well plates at 5 ×10^3 cells/well in at least triplicates. After 24 h, the cells were treated with 20 µM DGAT1 and 20 µM DGAT2 inhibitors and/or 1 µM PGE$_2$ and/or 10 nM hGX sPLA$_2$ as described above, and left in complete medium for 72 h. PGE$_2$ was replenished every 24 h by direct addition to the culture medium. In transient transfection experiments, the cells were seeded in complete medium on 48-well plates at 3 ×10^4 (MDA-MB-231/Luciferase-2A-RFP cells) or 1.5 ×10^4 (A549 cells) cells/well. After 24 h, the cells were washed and transfected with 0.250 µg plasmid DNA/well using 0.5 µL P3000 reagent and 1 µL Lipofectamine 3000 in OptiMEM medium, and incubated in RPMI-1640 (MDA-MB-231) or DMEM/F12 with 2 mM L-glutamine (A549)

containing 0.02% EFAF-BSA. After 6 h, the cells were treated with 10 nM recombinant hGX $sPLA_2$ in complete medium, with 25 μM (A549) or 50 μM (MDA-MB-231) indomethacin, 25 μM nordihydroguaiaretic acid, and/or 20 μM each of the T863 and PF-06424439 DGAT1 and DGAT2 inhibitors, respectively. A549 cell proliferation was determined after 48 h using the direct cell proliferation assay kits (CyQUANT; Invitrogen, USA). MDA-MB-231/Luciferase-2A-RFP cell proliferation was determined by measuring RFP fluorescence emission (excitation, 558 nm; emission, 583 nm) on a microplate reader (Infinite M1000; Tecan, Austria). The final data were obtained after subtracting the background signal of the blank samples that contained culture medium without cells.

Statistical analysis

Statistical analyses were performed using Prism 9.0.2 (GraphPad Software, USA). Unless otherwise indicated, the data are presented as means ±SEM of at least three independent experiments. Statistical significance was determined using t-tests, one-way or two-way ANOVA, followed by Bonferroni, Sidak or Tukey's multiple comparison tests. P values <0.05 were considered as statistically significant.

Acknowledgements

We are grateful to Ana Temprano Lopez, Petra Hruševar, Ana Kump, Ema Guštin, Belen Vilanova Baeza and Špela Koren for their technical help, Dr. Mojca Pavlin (University of Ljubljana, Slovenia), Dr. Brett McKinnon (Berne University Hospital, Switzerland), Dr. Merce Miranda (Joan XXIII University Hospital Tarragona, Spain) and Dr. Boris Rogelj (Jožef Stefan Institute, Slovenia) for kindly providing cell lines. We thank Dr. Chris Berrie for critical reading of the manuscript. This work was supported by a Young Researcher grant (1000-15-106) and a postdoctoral grant (Z3-2650) to E.J.J., a Research Programme grant (P1-0207) and a Research Project grant (J7-1818) to T.P., from the Slovenian Research Agency; by the Deutsche Forschungsgemeinschaft (DFG, German Research Foundation), Project-ID 239748522 - SFB 1127 ChemBioSys, and the EU COST Action CA19105 EpiLipidNet.

Author contributions

EJJ performed most of the experiments, analysed the data, and prepared the figures and initial manuscript drafts; APJ and VB performed initial lipidomic experiments; TOE and RZ performed mass spectrometry analyses, designed experiments, contributed ideas and revised the paper; GL contributed materials, ideas and revised the paper; PMJ, JG and OW performed lipid

mediator mass spectrometry analyses and revised the paper; TP conceptualised the study, analysed the data, prepared the figures and illustrations, and wrote the manuscript.

Conflicts of interest

The authors declare that they have no conflicts of interest.

References

Accioly MT, Pacheco P, Maya-Monteiro CM, Carrossini N, Robbs BK, Oliveira SS, Kaufmann C, Morgado-Diaz JA, Bozza PT & Viola JPB (2008) Lipid bodies are reservoirs of cyclooxygenase-2 and sites of prostaglandin E_2 synthesis in colon cancer cells. *Cancer Res* 68: 1732–1740

Ackerman D, Tumanov S, Qiu B, Michalopoulou E, Spata M, Azzam A, Xie H, Simon MC & Kamphorst JJ (2018) Triglycerides promote lipid homeostasis during hypoxic stress by balancing fatty acid saturation. *Cell Reports* 24: 2596–2605.e5

Ait-Oufella H, Herbin O, Lahoute C, Coatrieux C, Loyer X, Joffre J, Laurans L, Ramkhelawon B, Blanc-Brude O, Karabina S, *et al* (2013) Group X secreted phospholipase A_2 limits the development of atherosclerosis in LDL-receptor-null mice. *Arteriosclerosis Thrombosis Vasc Biology* 33: 466–473

Al-Zoughbi W, Pichler M, Gorkiewicz G, Guertl-Lackner B, Haybaeck J, Jahn SW, Lackner C, Liegl-Atzwanger B, Popper H, Schauer S, *et al* (2016) Loss of adipose triglyceride lipase is associated with human cancer and induces mouse pulmonary neoplasia. *Oncotarget* 7: 33832–33840.

Antonny B, Vanni S, Shindou H & Ferreira T (2015) From zero to six double bonds: phospholipid unsaturation and organelle function. *Trends Cell Biol* 25: 427–436

Astudillo AM, Balboa MA & Balsinde J (2019) Selectivity of phospholipid hydrolysis by phospholipase A_2 enzymes in activated cells leading to polyunsaturated fatty acid mobilization. *Biochim Biophys Acta - Mol Cell Biol Lipids* 1864: 772–783.

Bailey AP, Koster G, Guillermier C, Hirst EMA, MacRae JI, Lechene CP, Postle AD & Gould AP (2015) Antioxidant role for lipid droplets in a stem cell niche of *Drosophila*. *Cell* 163: 340–353

Bezzine S, Bollinger JG, Singer AG, Veatch SL, Keller SL & Gelb MH (2002) On the binding preference of human groups IIA and X phospholipases A_2 for membranes with anionic phospholipids. *J Biol Chem* 277: 48523–48534

Bonventre J (2004) Cytosolic phospholipase A_2alpha reigns supreme in arthritis and bone resorption. *Trends Immunol* 25, 116–119

Bosch M, Parton RG & Pol A (2020) Lipid droplets, bioenergetic fluxes, and metabolic flexibility. *Semin Cell Dev Biol* 108: 33–46

Bosch M, Sweet MJ, Parton RG & Pol A (2021) Lipid droplets and the host–pathogen dynamic: FATal attraction? *J Cell Biol* 220: e202104005

1147 Bozza PT, Bakker-Abreu I, Navarro-Xavier RA & Bandeira-Melo C (2011) Lipid body function
1148 in eicosanoid synthesis: an update. *Prostaglandins Leukot Essent Fatty Acids* 85: 205–
1149 213
1150 Brglez V, Lambeau G & Petan T (2014a) Secreted phospholipases A_2 in cancer: diverse
1151 mechanisms of action. *Biochimie* 107 Pt A: 114–23
1152 Brglez V, Pucer A, Pungerčar J, Lambeau G & Petan T (2014b) Secreted phospholipases A_2
1153 are differentially expressed and epigenetically silenced in human breast cancer cells.
1154 *Biochem Biophys Res Commun* 445: 230–235
1155 Brok MH den, Raaijmakers TK, Collado-Camps E & Adema GJ (2018) Lipid droplets as
1156 immune modulators in myeloid cells. *Trends Immunol* 39: 380–392
1157 Cao J, Zhou Y, Peng H, Huang X, Stahler S, Suri V, Qadri A, Gareski T, Jones J, Hahm S, *et*
1158 *al* (2011) Targeting acyl-CoA:diacylglycerol acyltransferase 1 (DGAT1) with small
1159 molecule inhibitors for the treatment of metabolic diseases. *J Biol Chem* 286: 41838–
1160 41851
1161 Cao Z, Hao Y, Fung CW, Lee YY, Wang P, Li X, Xie K, Lam WJ, Qiu Y, Tang BZ, *et al* (2019)
1162 Dietary fatty acids promote lipid droplet diversity through seipin enrichment in an ER
1163 subdomain. *Nat Commun* 10: 2902
1164 Castoldi A, Monteiro LB, Bakker N van T, Sanin DE, Rana N, Corrado M, Cameron AM,
1165 Hässler F, Matsushita M, Caputa G, *et al* (2020) Triacylglycerol synthesis enhances
1166 macrophage inflammatory function. *Nat Commun* 11: 4107
1167 Cheng X, Geng F, Pan M, Wu X, Zhong Y, Wang C, Tian Z, Cheng C, Zhang R, Puduvalli V,
1168 *et al* (2020) Targeting DGAT1 ameliorates glioblastoma by increasing fat catabolism and
1169 oxidative stress. *Cell Metab* 32: 229–242.e8
1170 Chitraju C, Mejhert N, Haas JT, Diaz-Ramirez LG, Grueter CA, Imbriglio JE, Pinto S, Koliwad
1171 SK, Walther TC & Farese RV (2017) Triglyceride synthesis by DGAT1 protects adipocytes
1172 from lipid-induced ER stress during lipolysis. *Cell Metab* 26: 407–418.e3
1173 Coleman RA & Mashek DG (2011) Mammalian triacylglycerol metabolism: synthesis, lipolysis,
1174 and signaling. *Chem Rev* 111: 6359–6386
1175 Cruz ALS, Barreto E de A, Fazolini NPB, Viola JPB & Bozza PT (2020) Lipid droplets: platforms
1176 with multiple functions in cancer hallmarks. *Cell Death Dis* 11: 105
1177 Dalli J & Serhan CN (2012) Specific lipid mediator signatures of human phagocytes:
1178 microparticles stimulate macrophage efferocytosis and pro-resolving mediators. *Blood*
1179 120: e60–e72
1180 Dennis EA & Norris PC (2015) Eicosanoid storm in infection and inflammation. *Nat Rev*
1181 *Immunol* 15: 511–523

1182 Dichlberger A, Schlager S, Maaninka K, Schneider WJ & Kovanen PT (2014) Adipose
1183 triglyceride lipase regulates eicosanoid production in activated human mast cells. *J Lipid*
1184 *Res* 55: 2471–2478
1185 Dierge E, Debock E, Guilbaud C, Corbet C, Mignolet E, Mignard L, Bastien E, Dessy C,
1186 Larondelle Y & Feron O (2021) Peroxidation of n-3 and n-6 polyunsaturated fatty acids in
1187 the acidic tumor environment leads to ferroptosis-mediated anticancer effects. *Cell Metab*
1188 33: 1701–1715.e5
1189 Dvorak AM, Dvorak HF, Peters SP, Shulman ES, MacGlashan DW, Pyne K, Harvey VS, Galli
1190 SJ & Lichtenstein LM (1983) Lipid bodies: cytoplasmic organelles important to
1191 arachidonate metabolism in macrophages and mast cells. *J Immunol* 131: 2965–2976
1192 Duchez A-C, Boudreau LH, Naika GS, Rousseau M, Cloutier N, Levesque T, Gelb MH &
1193 Boilard E (2019) Respective contribution of cytosolic phospholipase A2α and secreted
1194 phospholipase A_2 IIA to inflammation and eicosanoid production in arthritis. *Prostaglandins*
1195 *Other Lipid Mediat* 143: 106340
1196 Eichmann TO, Kumari M, Haas JT, Farese RV, Zimmermann R, Lass A & Zechner R (2012)
1197 Studies on the substrate and stereo/ regioselectivity of adipose triglyceride lipase,
1198 hormone-sensitive lipase, and diacylglycerol-O-acyltransferases. *J Biol Chem* 287:
1199 41446–41457
1200 Fishbein A, Hammock BD, Serhan CN & Panigrahy D (2020) Carcinogenesis: failure of
1201 resolution of inflammation? *Pharmacol Ther* 218: 107670
1202 Futatsugi K, Kung DW, Orr STM, Cabral S, Hepworth D, Aspnes G, Bader S, Bian J, Boehm
1203 M, Carpino PA, *et al* (2015) Discovery and optimization of imidazopyridine-based inhibitors
1204 of diacylglycerol acyltransferase 2 (DGAT2). *J Med Chem* 58: 7173–7185
1205 Gartung A, Zhao J, Chen S, Mottillo E, VanHecke GC, Ahn Y-H, Maddipati KR, Sorokin A,
1206 Granneman J & Lee M-J (2016) Characterization of eicosanoids produced by adipocyte
1207 lipolysis: implication of cyclooxygenase-2 in adipose inflammation. *J Biol Chem* 291:
1208 16001–16010
1209 Giedt MS, Thomalla JM, Johnson MR, Lai ZW, Tootle TL & Welte MA (2021) Lipid droplets
1210 regulate actin remodeling via prostaglandin signaling during *Drosophila* oogenesis.
1211 *bioRxiv* 2021.08.02.454724; doi: https://doi.org/10.1101/2021.08.02.454724 [PREPRINT]
1212 Greenberg AS, Coleman RA, Kraemer FB, McManaman JL, Obin MS, Puri V, Yan Q-W,
1213 Miyoshi H & Mashek DG (2011) The role of lipid droplets in metabolic disease in rodents
1214 and humans. *J Clin Invest* 121: 2102–2110
1215 Greene ER, Huang S, Serhan CN & Panigrahy D (2011) Regulation of inflammation in cancer
1216 by eicosanoids. *Prostag Other Lipid Mediat* 96: 27–36

1217 Gubern A, Casas J, Barceló-Torns M, Barneda D, Rosa X de la, Masgrau R, Picatoste F,
1218 Balsinde J, Balboa MA & Claro E (2008) Group IVA phospholipase A_2 is necessary for the
1219 biogenesis of lipid droplets. *J Biol Chem* 283: 27369–27382
1220 Guillaume C, Payré C, Jemel I, Jeammet L, Bezzine S, Naika GS, Bollinger J, Grellier P, Gelb
1221 MH, Schrével J, *et al* (2015) In vitro anti-*Plasmodium falciparum* properties of the full set
1222 of human secreted phospholipases A_2. *Infect Immun* 83: 2453–2465
1223 Guijas C, Rodríguez JP, Rubio JM, Balboa MA & Balsinde J (2014) Phospholipase A_2
1224 regulation of lipid droplet formation. *Biochim Biophys Acta* 1841: 1661–1671
1225 Haemmerle G, Moustafa T, Woelkart G, Büttner S, Schmidt A, Weijer T van de, Hesselink M,
1226 Jaeger D, Kienesberger PC, Zierler K, *et al* (2011) ATGL-mediated fat catabolism
1227 regulates cardiac mitochondrial function via PPAR-α and PGC-1. *Nat Med* 17: 1076–1085
1228 Hanasaki K, Ono T, Saiga A, Morioka Y, Ikeda M, Kawamoto K, Higashino K, Nakano K,
1229 Yamada K, Ishizaki J & Arita H (1999) Purified group X secretory phospholipase A_2 induced
1230 prominent release of arachidonic acid from human myeloid leukemia cells. *J Biol Chem*
1231 274: 34203–34211
1232 Hayashi D, Mouchlis VD & Dennis EA (2021) Omega-3 *versus* omega-6 fatty acid availability
1233 is controlled by hydrophobic site geometries of phospholipase A_2s. *J Lipid Res* 62: 100113
1234 doi: 10.1016/j.jlr.2021.100113 [paper in press]
1235 Henne WM, Reese ML & Goodman JM (2018) The assembly of lipid droplets and their roles
1236 in challenged cells. *EMBO J* 37: e98947
1237 Jarc E, Kump A, Malavašič P, Eichmann TO, Zimmermann R & Petan T (2018) Lipid droplets
1238 induced by secreted phospholipase A_2 and unsaturated fatty acids protect breast cancer
1239 cells from nutrient and lipotoxic stress. *Biochim Biophys Acta - Mol Cell Biol Lipids* 1863:
1240 247–265
1241 Jarc E & Petan T (2020) A twist of FATe: lipid droplets and inflammatory lipid mediators.
1242 *Biochimie* 169: 69–87
1243 Koizume S & Miyagi Y (2016) Lipid droplets: a key cellular organelle associated with cancer
1244 cell survival under normoxia and hypoxia. *Int J Mol Sci* 17: 1430
1245 Koliwad SK, Streeper RS, Monetti M, Cornelissen I, Chan L, Terayama K, Naylor S, Rao M,
1246 Hubbard B & Farese RV (2010) DGAT1-dependent triacylglycerol storage by
1247 macrophages protects mice from diet-induced insulin resistance and inflammation. *J Clin*
1248 *Invest* 120: 756–767
1249 Koundouros N, Karali E, Tripp A, Valle A, Inglese P, Perry NJS, Magee DJ, Virmouni SA, Elder
1250 GA, Tyson AL, *et al* (2020) Metabolic fingerprinting links oncogenic PIK3CA with enhanced
1251 arachidonic-acid-derived eicosanoids. *Cell* 181: 1596–1611.e27
1252 Krahmer N, Farese RV & Walther TC (2013) Balancing the fat: lipid droplets and human
1253 disease. *EMBO Mol Med* 5: 905–915

1254 Lambeau G & Gelb MH (2008) Biochemistry and physiology of mammalian secreted
1255 phospholipases A_2. *Annu Rev Biochem* 77: 495–520
1256 Leslie CC (2015) Cytosolic phospholipase A_2: physiological function and role in disease. *J Lipid*
1257 *Res* 56: 1386–1402
1258 Li X, Shridas P, Forrest K, Bailey W & Webb NR (2010) Group X secretory phospholipase A_2
1259 negatively regulates adipogenesis in murine models. *FASEB J* 24: 4313–4324
1260 Liesenfeld DB, Grapov D, Fahrmann JF, Salou M, Scherer D, Toth R, Habermann N, Bohm J,
1261 Schrotz-King P, Gigic B, *et al* (2015) Metabolomics and transcriptomics identify pathway
1262 differences between visceral and subcutaneous adipose tissue in colorectal cancer
1263 patients: the ColoCare study. *Am J Clin Nutrition* 102: 433–443
1264 Listenberger LL, Han X, Lewis SE, Cases S, Farese RV, Ory DS & Schaffer JE (2003)
1265 Triglyceride accumulation protects against fatty acid-induced lipotoxicity. *Proc Natl Acad*
1266 *Sci U S A* 100: 3077–3082
1267 Molenaar MR, Jeucken A, Wassenaar TA, van de Lest CHA, Brouwers JF & Helms JB (2019)
1268 LION/web: a web-based ontology enrichment tool for lipidomic data analysis. *Gigascience*
1269 8: giz061
1270 Moreira LS, Piva B, Gentile LB, Mesquita-Santos FP, D'Avila H, Maya-Monteiro CM, Bozza
1271 PT, Bandeira-Melo C & Diaz BL (2009) Cytosolic phospholipase A_2-driven PGE2 synthesis
1272 within unsaturated fatty acids-induced lipid bodies of epithelial cells. *Biochim Biophys Acta*
1273 *- Mol Cell Biology Lipids* 1791: 156–165
1274 Mounier CM, Ghomashchi F, Lindsay MR, James S, Singer AG, Parton RG & Gelb MH (2004)
1275 Arachidonic acid release from mammalian cells transfected with human groups IIA and X
1276 secreted phospholipase A_2 occurs predominantly during the secretory process and with
1277 the involvement of cytosolic phospholipase A_2-α. *J Biol Chem* 279: 25024–25038
1278 Murakami M (2017) Lipoquality control by phospholipase A_2 enzymes. *Proc Jpn Acad Ser B*
1279 93: 677–702
1280 Murakami M, Sato H & Taketomi Y (2020) Updating phospholipase A_2 biology. *Biomolecules*
1281 10: 1457
1282 Murakami M, Taketomi Y, Miki Y, Sato H, Hirabayashi T & Yamamoto K (2011) Recent
1283 progress in phospholipase A_2 research: from cells to animals to humans. *Prog Lipid Res*
1284 50: 152–192
1285 Murase R, Sato H, Yamamoto K, Ushida A, Nishito Y, Ikeda K, Kobayashi T, Yamamoto T,
1286 Taketomi Y & Murakami M (2016) Group X secreted phospholipase A_2 releases ω3
1287 polyunsaturated fatty acids, suppresses colitis, and promotes sperm fertility. *J Biol Chem*
1288 291: 6895–6911

1289 Nguyen TB, Louie SM, Daniele JR, Tran Q, Dillin A, Zoncu R, Nomura DK & Olzmann JA
1290 (2017) DGAT1-dependent lipid droplet biogenesis protects mitochondrial function during
1291 starvation-induced autophagy. *Dev Cell* 42: 9–21.e5
1292 Nieman KM, Kenny HA, Penicka CV, Ladanyi A, Buell-Gutbrod R, Zillhardt MR, Romero IL,
1293 Carey MS, Mills GB, Hotamisligil GS, *et al* (2010) Adipocytes promote ovarian cancer
1294 metastasis and provide energy for rapid tumor growth. *Nat Med* 17: 1498–1503
1295 Nomura DK, Lombardi DP, Chang JW, Niessen S, Ward AM, Long JZ, Hoover HH & Cravatt
1296 BF (2011) Monoacylglycerol lipase exerts dual control over endocannabinoid and fatty acid
1297 pathways to support prostate cancer. *Chem Biol* 18: 846–856
1298 Nomura DK, Long JZ, Niessen S, Hoover HS, Ng S-W & Cravatt BF (2010) Monoacylglycerol
1299 lipase regulates a fatty-acid network that promotes cancer pathogenesis. *Cell* 140: 49–61
1300 Ogden HL, Lai Y, Nolin JD, An D, Frevert CW, Gelb MH, Altemeier WA & Hallstrand TS (2020)
1301 Secreted phospholipase A_2 group X acts as an adjuvant for type 2 inflammation, leading
1302 to an allergen-specific immune response in the lung. *J Immunol* 204: 3097–3107
1303 Olzmann JA & Carvalho P (2019) Dynamics and functions of lipid droplets. *Nat Rev Mol Cell*
1304 *Biology* 20: 137–155
1305 Paar M, Jungst C, Steiner NA, Magnes C, Sinner F, Kolb D, Lass A, Zimmermann R,
1306 Zumbusch A, Kohlwein SD, *et al* (2012) Remodeling of lipid droplets during lipolysis and
1307 growth in adipocytes. *J Biol Chem* 287: 11164–11173
1308 Pavlova NN & Thompson CB (2016) The emerging hallmarks of cancer metabolism. *Cell*
1309 *Metab* 23: 27–47
1310 Pereira-Dutra FS, Teixeira L, Costa MFS & Bozza PT (2019) Fat, fight, and beyond: the
1311 multiple roles of lipid droplets in infections and inflammation. *J Leukocyte Biol* 106: 563–
1312 580
1313 Pérez-Chacón G, Astudillo AM, Balgoma D, Balboa MA & Balsinde J (2009) Control of free
1314 arachidonic acid levels by phospholipases A_2 and lysophospholipid acyltransferases.
1315 *Biochim Biophys Acta - Mol Cell Biology Lipids* 1791: 1103–1113
1316 Petan T (2020) Lipid droplets in cancer. *Rev Physiol Biochem Pharmacol.* Springer, Berlin,
1317 Heidelberg. https://doi.org/10.1007/112_2020_51 [paper in press]
1318 Pucer A, Brglez V, Payré C, Pungerčar J, Lambeau G & Petan T (2013) Group X secreted
1319 phospholipase A_2 induces lipid droplet formation and prolongs breast cancer cell survival.
1320 *Mol Cancer* 12: 111
1321 Rambold AS, Cohen S & Lippincott-Schwartz J (2015) Fatty-acid trafficking in starved cells:
1322 regulation by lipid droplet lipolysis, autophagy, and mitochondrial fusion dynamics. *Dev*
1323 *Cell* 32: 678–692

1324 Riederer M, Lechleitner M, Köfeler H & Frank S (2017) Reduced expression of adipose
1325 triglyceride lipase decreases arachidonic acid release and prostacyclin secretion in human
1326 aortic endothelial cells. *Arch Physiol Biochem* 123: 249–253
1327 Röhrig F & Schulze A (2016) The multifaceted roles of fatty acid synthesis in cancer. *Nat Rev*
1328 *Cancer* 16: 732–749
1329 Saiga A, Uozumi N, Ono T, Seno K, Ishimoto Y, Arita H, Shimizu T & Hanasaki K (2005) Group
1330 X secretory phospholipase A2 can induce arachidonic acid release and eicosanoid
1331 production without activation of cytosolic phospholipase A2 alpha. *Prostaglandins Other*
1332 *Lipid Mediat* 75: 79–89
1333 Sato H, Isogai Y, Masuda S, Taketomi Y, Miki Y, Kamei D, Hara S, Kobayashi T, Ishikawa Y,
1334 Ishii T, *et al* (2011) Physiological roles of group X-secreted phospholipase A_2 in
1335 reproduction, gastrointestinal phospholipid digestion, and neuronal function. *J Biol Chem*
1336 286: 11632–11648
1337 Sato H, Taketomi Y, Miki Y, Murase R, Yamamoto K & Murakami M (2020) Secreted
1338 phospholipase PLA2G2D contributes to metabolic health by mobilizing ω3
1339 polyunsaturated fatty acids in WAT. *Cell Reports* 31: 107579
1340 Schewe M, Franken PF, Sacchetti A, Schmitt M, Joosten R, Böttcher R, Royen ME van,
1341 Jeammet L, Payré C, Scott PM, *et al* (2016) Secreted phospholipases A_2 are intestinal
1342 stem cell niche factors with distinct roles in homeostasis, inflammation, and cancer. *Cell*
1343 *Stem Cell* 19: 38–51
1344 Schlager S, Goeritzer M, Jandl K, Frei R, Vujic N, Kolb D, Strohmaier H, Dorow J, Eichmann
1345 TO, Rosenberger A, *et al* (2015) Adipose triglyceride lipase acts on neutrophil lipid droplets
1346 to regulate substrate availability for lipid mediator synthesis. *J Leukocyte Biol* 98: 837–850
1347 Schlager S, Vujic N, Korbelius M, Duta-Mare M, Dorow J, Leopold C, Rainer S, Wegscheider
1348 M, Reicher H, Ceglarek U, *et al* (2017) Lysosomal lipid hydrolysis provides substrates for
1349 lipid mediator synthesis in murine macrophages. *Oncotarget* 8: 40037–40051
1350 Schott MB, Weller SG, Schulze RJ, Krueger EW, Drizyte-Miller K, Casey CA & McNiven MA
1351 (2019) Lipid droplet size directs lipolysis and lipophagy catabolism in hepatocytes. *J Cell*
1352 *Biol* 218: 3320–3335
1353 Schuldiner M & Bohnert M (2017) A different kind of love - lipid droplet contact sites. *Biochim*
1354 *Biophys Acta* 1862: 1188–1196
1355 Schweiger M, Romauch M, Schreiber R, Grabner GF, Hütter S, Kotzbeck P, Benedikt P,
1356 Eichmann TO, Yamada S, Knittelfelder O, *et al* (2017) Pharmacological inhibition of
1357 adipose triglyceride lipase corrects high-fat diet-induced insulin resistance and
1358 hepatosteatosis in mice. *Nat Commun* 8: 14859
1359 Serhan CN (2014) Pro-resolving lipid mediators are leads for resolution physiology. *Nature*
1360 510: 92–101

1361 Shimizu T (2009) Lipid mediators in health and disease: enzymes and receptors as therapeutic
1362 targets for the regulation of immunity and inflammation. *Annu Rev Pharmacol* 49: 123–150
1363 Shridas P, Bailey WM, Boyanovsky BB, Oslund RC, Gelb MH & Webb NR (2010) Group X
1364 secretory phospholipase A_2 regulates the expression of steroidogenic acute regulatory
1365 protein (StAR) in mouse adrenal glands. *J Biol Chem* 285: 20031–20039
1366 Slatter DA, Aldrovandi M, O'Connor A, Allen SM, Brasher CJ, Murphy RC, Mecklemann S,
1367 Ravi S, Darley-Usmar V & O'Donnell VB (2016) Mapping the human platelet lipidome
1368 reveals cytosolic phospholipase A_2 as a regulator of mitochondrial bioenergetics during
1369 activation. *Cell Metab* 23: 930–944
1370 Smirnova E, Goldberg EB, Makarova KS, Lin L, Brown WJ & Jackson CL (2005) ATGL has a
1371 key role in lipid droplet/adiposome degradation in mammalian cells. *EMBO Rep* 7: 106–
1372 113
1373 Sohn JH, Lee YK, Han JS, Jeon YG, Kim JI, Choe SS, Kim SJ, Yoo HJ & Kim JB (2018)
1374 Perilipin 1 (Plin1) deficiency promotes inflammatory responses in lean adipose tissue
1375 through lipid dysregulation. *J Biol Chem* 293: 13974–13988
1376 Sulciner ML, Serhan CN, Gilligan MM, Mudge DK, Chang J, Gartung A, Lehner KA, Bielenberg
1377 DR, Schmidt B, Dalli J, *et al* (2018) Resolvins suppress tumor growth and enhance cancer
1378 therapy. *J Exp Med* 215: 115–140
1379 Surrel F, Jemel I, Boilard E, Bollinger JG, Payré C, Mounier CM, Talvinen KA, Laine VJO,
1380 Nevalainen TJ, Gelb MH, *et al* (2009) Group X phospholipase A_2 stimulates the
1381 proliferation of colon cancer cells by producing various lipid mediators. *Mol Pharmacol* 76:
1382 778–790
1383 Thiam AR & Ikonen E (2020) Lipid droplet nucleation. *Trends Cell Biol* 31: 108–118
1384 Triggiani M, Oriente A & Marone G (1994) Differential roles for triglyceride and phospholipid
1385 pools of arachidonic acid in human lung macrophages. *J Immunol* 152: 1394–1403
1386 Walther TC, Chung J & Farese RV (2017) Lipid droplet biogenesis. *Annu Rev Cell Dev Biol*
1387 33: 491–510
1388 Wang D & DuBois RN (2010) Eicosanoids and cancer. *Nat Rev Cancer* 10: 181–193
1389 Wang YY, Attané C, Milhas D, Dirat B, Dauvillier S, Guerard A, Gilhodes J, Lazar I, Alet N,
1390 Laurent V, *et al* (2017) Mammary adipocytes stimulate breast cancer invasion through
1391 metabolic remodeling of tumor cells. *JCI Insight* 2: e87489
1392 Ward KE, Ropa JP, Adu-Gyamfi E & Stahelin RV (2012) C2 domain membrane penetration by
1393 group IVA cytosolic phospholipase A_2 induces membrane curvature changes. *J Lipid Res*
1394 53: 2656–2666
1395 Ward KE, Sengupta R, Ropa JP, Amiar S & Stahelin ARV (2020) The cytosolic phospholipase
1396 $A_2\alpha$ N-terminal C2 domain binds and oligomerizes on membranes with positive curvature.
1397 *Biomolecules* 10: 647

Welte MA & Gould AP (2017) Lipid droplet functions beyond energy storage. *Biochim Biophys Acta* 1862: 1260–1272

Werner M, Jordan PM, Romp E, Czapka A, Rao Z, Kretzer C, Koeberle A, Garscha U, Pace S, Claesson H, *et al* (2019) Targeting biosynthetic networks of the proinflammatory and proresolving lipid metabolome. *FASEB J* 33: 6140–6153

Werz O, Gerstmeier J, Libreros S, Rosa XD la, Werner M, Norris PC, Chiang N & Serhan CN (2018) Human macrophages differentially produce specific resolvin or leukotriene signals that depend on bacterial pathogenicity. *Nat Commun* 9: 59

Wilcock DJ, Badrock AP, Owen R, Guerin M, Southam AD, Johnston H, Ogden S, Fullwood P, Watson J, Ferguson H, *et al* (2020) DGAT1 is a lipid metabolism oncoprotein that enables cancer cells to accumulate fatty acid while avoiding lipotoxicity. bioRxiv 2020.06.23.166603; doi: https://doi.org/10.1101/2020.06.23.166603 [PREPRINT]

Wooten RE, Willingham MC, Daniel LW, Leslie CC, Rogers LC, Sergeant S & O'Flaherty JT (2008) Novel translocation responses of cytosolic phospholipase $A_2\alpha$ fluorescent proteins. *Biochim Biophys Acta* 1783: 1544–1550

Yin H, Li W, Mo L, Deng S, Lin W, Ma C, Luo Z, Luo C & Hong H (2021) Adipose triglyceride lipase promotes the proliferation of colorectal cancer cells via enhancing the lipolytic pathway. *J Cell Mol Med* 25: 3963–3975

Zagani R, El-Assaad W, Gamache I & Teodoro JG (2015) Inhibition of adipose triglyceride lipase (ATGL) by the putative tumor suppressor G0S2 or a small molecule inhibitor attenuates the growth of cancer cells. *Oncotarget* 6: 28282–28295

Zechner R, Madeo F & Kratky D (2017) Cytosolic lipolysis and lipophagy: two sides of the same coin. *Nat Rev Mol Cell Biol* 18: 671–684

Zechner R, Zimmermann R, Eichmann TO, Kohlwein SD, Haemmerle G, Lass A & Madeo F (2012) FAT SIGNALS - Lipases and lipolysis in lipid metabolism and signaling. *Cell Metab* 15: 279–291

Zimmermann R, Strauss JG, Haemmerle G, Schoiswohl G, Birner-Gruenberger R, Riederer M, Lass A, Neuberger G, Eisenhaber F, Hermetter A, *et al* (2004) Fat mobilization in adipose tissue is promoted by adipose triglyceride lipase. *Science* 306: 1383–1386

Zoni V, Khaddaj R, Campomanes P, Thiam AR, Schneiter R & Vanni S (2021) Pre-existing bilayer stresses modulate triglyceride accumulation in the ER *versus* lipid droplets. *Elife* 10: e62886

Figure legends

Figure 1. $sPLA_2$ promotes enrichment of lipid droplets with long-chain PUFA-containing triglycerides. (**A, B**) Lipid droplet levels in control cells and cells treated with 10 nM recombinant hGX $sPLA_2$ for 48 h in serum-rich medium. (**A**) Neutral lipid content was quantified by Nile Red staining and flow cytometry (n = 3 independent experiments; 20000 cells per treatment). (**B**) Representative live-cell confocal microscopy imaging of lipid droplets stained with BODIPY 493/503 (green) and nuclei with Hoechst 33342 (blue). (**C**) Diagram illustrating the hypothesis that unsaturated fatty acids released through $sPLA_2$ membrane hydrolysis are incorporated into triacylglycerols (TAGs) and lead to lasting changes in lipid droplet TAG acyl-chain composition. (**D**) hGX-$sPLA_2$-induced changes in the incorporation of radiolabelled oleate into cellular TAGs in MDA-MB-231 cells grown in complete medium for 24 h (Fed), in complete medium for 24 h followed by 96 h of serum starvation (Fed + Starved), and in serum-free medium for 96 h (Starved) (n = 4 independent experiments). (**E**) Diagram illustrating the experimental treatments used for lipidomic analysis in (F)–(K). (**F–K**) TAG lipidomic analyses of MDA-MB-231 cells treated with recombinant hGX $sPLA_2$ in complete medium for 48 h (Fed; F–H, J, K) or in the absence of serum for 96 h (Starved; F, I). Cell lysates were collected and analysed by UPLC/qTOF-MS (n = 4 independent experiments). (**G–I**) $sPLA_2$-induced changes in the levels of individual TAG species presented as a representative z-score heat-map (**G**) and volcano plots (**H, I**) prepared by $\log_2$ data transformation and multiple t-test analyses (n = 4 independent experiments). Statistically significant changes ($-\log_{10}$(P value) > 1.30) in TAGs containing mostly saturated and mono-unsaturated FAs (SFA/MUFA-TAGs with 0–2 double bonds; blue) and those containing polyunsaturated FAs (PUFA-TAGs with 3–12 double bonds; red) are shown. (**J, K**) $sPLA_2$-induced changes in relative levels of TAG species grouped by number of acyl-chain C-atoms (chain length) and double bonds (chain unsaturation). (**A–K**) Data are means ±SEM of at least three independent experiments. *, P <0.05; **, P <0.01; ***, P <0.001 (unpaired t-tests).

Figure 2. ATGL-mediated lipid droplet breakdown is required for PGE_2 production in serum-starved cancer cells. (**A**) Diagram illustrating the experimental set-up used to load cells with lipid droplets (Feeding) and then to induce their breakdown (Starvation). (**B**) PGE_2 levels in cell supernatants of control and hGX-$sPLA_2$-treated cells quantified by ELISA at the end of the starvation period. (**C**) Diagram illustrating the experimental conditions used in (D)–(F) and Fig. EV1(E)–(O). (**D, E**) Lipid droplet levels and PGE_2 production in ATGL-silenced control and $sPLA_2$-treated cells grown as shown in (C) and analysed at the beginning (Fed) and at the end of the serum starvation period (Fed + Starved). Neutral lipids were quantified

by Nile Red staining and flow cytometry, PGE_2 was quantified by ELISA. (**F**) Representative confocal microscopy images showing effects of ATGL depletion on cellular lipid droplet content in control and hGX-$sPLA_2$-treated cells, under serum-rich (Fed) and serum-free (Fed + Starved) conditions. Lipid droplets and nuclei were stained using BODIPY 493/503 and Hoechst 33342, respectively. (**G**) Diagram illustrating the experimental set-up used in (H), (I) and Figure EV1P, R. (**H, I**) Glycerol release and PGE_2 production in ATGL-overexpressing serum-starved cells (both untreated and hGX $sPLA_2$ pretreated), in comparison with cells co-transfected with ATGL-specific siRNAs ($ATGL^{KD+OE}$), non-targeting siRNA (scrambled) and control plasmid (empty), grown as illustrated in (G). (**J**) Diagram illustrating the proposed model of lipid droplet-mediated eicosanoid production in cancer cells. Data are means ±SEM of two (H) or three (B–E, I) independent experiments. *, P <0.05; **, P <0.01; ***, P <0.001 (two-way ANOVA with Tukey (I) or Bonferroni (D, E, H) adjustment; unpaired t-tests (B)).

Figure 3. ATGL-mediated lipolysis drives production of a wide spectrum of bioactive lipid mediators. (**A–D**) Comparative analysis of the profiles of lipid mediators released from serum-starved MDA-MB-231 cells pre-treated with hGX $sPLA_2$, and from ATGL-depleted cells without and with hGX $sPLA_2$ pre-treatment, presented as volcano plots (A) a heat map (B), and individual graphs (C, D). Cells were treated as shown in Fig. 2C. Volcano plots were prepared using log_2-transformed fold-change values and multiple t-test analysis, and the heat map by –logP data transformation and two-way ANOVA with Sidak adjustment (n = 3 independent experiments). (**E**) Diagram illustrating the involvement of hGX $sPLA_2$ and ATGL in the production of a wide range of PUFA-derived cyclooxygenase (COX) and lipoxygenase (LOX) signalling molecules. Data are means ±SEM of three independent experiments. *, P <0.05; **, P <0.01; ***, P <0.001 (two-way ANOVA with Sidak adjustment).

Figure 4. Lipid droplets are required for PGE_2 production in serum-starved cancer cells. (**A**) Diagram illustrating the experimental conditions used (top) and cellular neutral lipid content before (Fed) and after (Fed + Starved) serum starvation in cells treated with DGAT1 (T863) and DGAT2 (PF-06427878) inhibitors (DGATi), without and with stimulation of lipid droplet biogenesis by hGX $sPLA_2$ during serum starvation. (**B**) Representative confocal microscopy images of live cells under nutrient-replete conditions and treated with DGAT inhibitors in the absence and presence of hGX $sPLA_2$. Lipid droplets and nuclei were visualised using BODIPY 493/503 and Hoechst 33342 staining, respectively, and confocal microscopy. (**C**) DGATi-induced changes in PGE_2 production in serum-starved cancer cells (Fed + Starved), without and with additional stimulation of lipid droplet biogenesis by hGX $sPLA_2$ pre-treatment. Cells were treated according to (A). (**D, E**) DGATi-induced changes in neutral lipids (D) and PGE_2 production (E) in serum-starved MDA-MB-231 cancer cells (Fed + Starved), without and with

additional stimulation of lipid droplet biogenesis by arachidonic acid (AA) pre-treatment. Cells were treated according to (A). (**F, G**) Diagrams illustrating the experimental conditions used (top), and changes in neutral lipid accumulation and PGE_2 production induced by DGATi treatments during serum starvation in control (SCR) and ATGL-depleted ($ATGL^{KD}$) MDA-MB-231 (F) and A549 (G) cancer cells, without and with hGX $sPLA_2$ pre-treatment. (**A, D, F, G**) Neutral lipid content was quantified by Nile Red staining and flow cytometry. (**C, E, F, G**) PGE_2 levels were determined in cell supernatants as described in Methods. Data are means ±SEM of at least three independent experiments. *, P <0.05; **, P <0.01; ***, P <0.001 (two-way ANOVA with Tukey (**A, F, G**) or Bonferroni (**C, D, E**) adjustment).

Figure 5. $cPLA_2\alpha$ depends on lipid droplet turnover to drive lipid mediator production. (**A**) Scheme illustrating three hypothetical models of interplay between $cPLA_2\alpha$ and ATGL in providing arachidonic acid (AA) for lipid mediator production. (**B**) Changes in neutral lipid content and PGE_2 production induced by ATGL ($ATGL^{KD}$) and $cPLA_2\alpha$ ($cPLA_2\alpha^{KD}$) single and double ($Double^{KD}$) knockdowns, in comparison with control siRNA-treated cells (SCR), without and with stimulation of lipid droplet biogenesis by hGX $sPLA_2$ pre-treatment. (**C**) PGE_2 production in cells with reciprocal knockdown/overexpression of $cPLA_2\alpha$ and ATGL. Cells were reverse transfected with siRNAs specific for ATGL ($ATGL^{KD}$) and/or $cPLA_2\alpha$ ($cPLA_2\alpha^{KD}$), then forward transfected with ATGL-encoding ($ATGL^{OE}$) and/or $cPLA_2\alpha$-encoding ($cPLA_2\alpha^{OE}$) plasmids, without and with pre-treated with hGX $sPLA_2$, as illustrated in the scheme (top). In controls (control), non-targeting siRNA reverse transfections were combined with backbone ('empty') vector forward transfections. (**D**) DGAT inhibition (DGATi)-induced changes in PGE_2 production in serum-starved control cells (empty) and in cells overexpressing ATGL ($ATGL^{OE}$) or $cPLA_2\alpha$ ($cPLA_2\alpha^{OE}$), without and with additional stimulation of lipid droplet biogenesis by hGX $sPLA_2$ pre-treatment. Neutral lipid content was quantified by Nile Red staining and flow cytometry (B), PGE_2 levels were determined in cell supernatants using ELISA (C, D). Data are means ±SEM of two (B, A549 cells) or at least three independent experiments *, P <0.05; **, P <0.01; ***, P <0.001 (two-way ANOVA with Tukey (B, D) or Dunnet (C) adjustment).

Figure 6. $cPLA_2\alpha$ affects lipid droplet turnover. (**A**) Diagram illustrating the experimental conditions used (top) and representative live-cell confocal microscopy imaging of lipid droplets in ATGL ($ATGL^{KD}$) and $cPLA_2\alpha$ ($cPLA_2\alpha^{KD}$) single and double ($Double^{KD}$) knockdown MDA-MB-231 cells, in comparison with control siRNA-treated cells (SCR), without and with stimulation of lipid droplet biogenesis by hGX $sPLA_2$ pre-treatment. The corresponding microscopy images for HeLa and A549 cells are shown in Figure EV4A, C. Lipid droplets were stained with BODIPY 493/503 (green) and nuclei with Hoechst 33342 (blue) and images analysed using ImageJ and the Lipid Droplet Counter Plugin. (**B**) Box plots and curves showing

changes in lipid droplet diameters in cells treated as in (A) (n >40 cells/sample). (**C–E**) Lipid droplet numbers per cell in serum-fed (Fed) and serum-starved (Starved) cells (n >40 cells/sample) grown and treated as in (A). Data are geometric means (B) or means (C–E) ±SEM (n >40 cells/sample) of two independent experiments. *, P <0.05; **, P <0.01; ***, P <0.001 (two-way ANOVA with Tukey adjustment; nested one-way ANOVA with Sidak adjustment (B)).

Figure 7. ATGL and cPLA$_2$α cooperatively modulate PUFA trafficking between triglycerides and membrane phospholipids. (**A–C**) Untargeted lipidomic analysis of phospholipids and triglycerides (TAGs) in serum-starved MDA-MB-231 cells depleted of ATGL (ATGL^{KD}), cPLA$_2$α (cPLA$_2$α^{KD}), or both (Double^{KD}), without and with hGX sPLA$_2$ pre-treatment under serum-rich conditions, and grown as shown in Figure EV5B. Volcano plots show significant changes (–log$_{10}$(P value) >1.30) in individual lipids between each treatment condition *versus* control cells (unless otherwise indicated), and were prepared by log$_2$ fold-change (FC) data transformation and multiple t-test analysis (n=3 independent experiments). TAGs and phospholipids (PLs) containing saturated and mono-unsaturated acyl chains (SFA/MUFA-TAGs, SFA/MUFA-PLs, with 0–3 and 0–2 double bonds, respectively) and those containing polyunsaturated FAs (PUFA-TAGs, PUFA-PLs, with at least 4 and 3 double bonds, respectively) are colour-coded as indicated. TG, triglyceride; PC, phosphatidylcholine; PE, phosphatidylethanolamine; PI, phosphatidylinositol, PS, phosphatidylserine. (**D**) Schematic illustration of the predominant pathways involved in lipid droplet-mediated PUFA trafficking between the membrane phospholipid and TAG pools in serum-starved cancer cells.

Figure 8. Lipid droplet-mediated lipid mediator production promotes cancer-cell proliferation. (**A**) Proliferation of MDA-MB-231 cells treated with T863 (DGAT1i) and PF-06427878 (DGAT2i), or an equimolar mix of both DGAT inhibitors (DGATi), grown under nutrient-rich conditions in the absence and presence of hGX sPLA$_2$. (**B, C**) Proliferation of MDA-MB-231 cells overexpressing ATGL (ATGL^{OE}), treated with indomethacin (B) or nordihydroguaiaretic acid (NDGA) (C), in the absence and presence of hGX sPLA$_2$. (**D**) Proliferation of MDA-MB-231 cells treated with exogenous PGE$_2$ in the absence and presence of T863 (DGAT1i) and PF-06427878 (DGAT2i), or an equimolar mix of both DGAT inhibitors (DGATi). (**E**) Proliferation of A549 cells overexpressing cPLA$_2$α (cPLA$_2$α^{OE}) and grown in the absence and presence of DGATi, indomethacin and recombinant hGX sPLA$_2$. (**F**) Proliferation of MDA-MB-231 cells overexpressing cPLA$_2$α (cPLA$_2$α^{OE}) and grown in the absence and presence of DGATi and recombinant hGX sPLA$_2$. Data are means ±SEM of three independent experiments. *, P <0.05; **, P <0.01; ***, P <0.001 (two-way ANOVA with Bonferroni (A–D) or Sidak (E, F) adjustments).

Expanded View Figure legends

Figure EV1. ATGL-mediated lipid droplet breakdown drives PGE_2 production in starving MDA-MB-231 and HeLa cells, but not in A549 cells. (**A, B**) Neutral lipid contents in control and hGX-sPLA$_2$-treated cells at the beginning of and after serum starvation, quantified by Nile Red staining and flow cytometry. (**C**) Glycerol released from fed and starving control and hGX-sPLA$_2$-treated cells. (**D**) PGE_2 levels in cell supernatants of control and AA-treated cells quantified by ELISA at the end of the starvation period. (**E**) Representative western blot showing siRNA-induced ATGL knock down (ATGL^{KD}) in comparison with control cells (untransfected [untr.] and non-targeting siRNA-transfected [SCR] cells), treated with hGX sPLA$_2$ (or left untreated) and grown as shown in (Fig. 2C). (**F, G, I, J**) Lipid droplet levels and PGE_2 production in ATGL-silenced control and sPLA$_2$-treated cells grown as shown in Fig. 2C and analysed at the beginning (Fed) and at the end of the serum starvation period (Fed + Starved). Neutral lipids were quantified by Nile Red staining and flow cytometry, PGE_2 was quantified by ELISA. (**H, K**) Representative confocal microscopy images showing effects of ATGL depletion on cellular lipid droplet content in control and hGX-sPLA$_2$-treated cells, under serum-rich (Fed) and serum-free (Fed + Starved) conditions. Lipid droplets and nuclei were stained using BODIPY 493/503 and Hoechst 33342, respectively. (**L, M**) Changes in lipid droplet levels and PGE_2 production induced by ATGL silencing in control and arachidonic acid (AA)-treated cells at the beginning (Fed) and end of the serum starvation (Fed + Starved). (**N, O**) Glycerol release as a measure of lipolytic activity in control and ATGL-depleted serum-fed and serum-starved cells, either untreated or treated with hGX sPLA$_2$. (**P**) Representative Western blot showing ATGL protein overexpression in cells transfected with ATGL-encoding plasmid (ATGL^{OE}) in comparison with those transfected with control (Empty) vector or ATGL-specific siRNA (ATGL^{KD}), grown as illustrated in Fig. 3J. (**R**) Neutral lipid levels in ATGL-overexpressing in untreated and hGX-sPLA$_2$-pretreated serum-starved cells, in comparison with those co-transfected with ATGL-specific siRNA (ATGL^{KD+OE}), non-targeting siRNA (scrambled) and control plasmid (empty), grown as shown in Fig. 2G. Neutral lipids were quantified by Nile Red staining and flow cytometry. Data are means ±SEM of two (D) or three (A–C, F, G, I, J, L–O) independent experiments. *, P <0.05; **, P <0.01; ***, P <0.001 (two-way ANOVA with Bonferroni (F, G, I, J, L–O) or Tukey (A, C, R) adjustment; unpaired t-test (D)).

Figure EV2. Inhibition of DGAT-mediated lipid droplet biogenesis supresses PGE_2 production. (**A, B**) Diagrams illustrating the experimental conditions used (top) and representative live-cell confocal microscopy images of control (SCR) and ATGL-depleted

(ATGL^{KD}) MDA-MB-231 and HeLa cells treated with DGAT inhibitors during serum feeding (A) and during serum starvation (B), without and with hGX sPLA$_2$ pre-treatment. Lipid droplets and nuclei were visualised using BODIPY 493/503 and Hoechst 33342 staining and confocal microscopy. (**C**) Diagram illustrating the experimental conditions (top) and graph showing DGAT inhibition (DGATi)-induced changes in PGE$_2$ production in serum-starved control (SCR) and ATGL-depleted (ATGL^{KD}) A549 cells, without and with stimulation of lipid droplet biogenesis by hGX sPLA$_2$ pre-treatment. PGE$_2$ levels were determined in cell supernatants as described in Methods. Data are means ±SEM of three independent experiments. *, P <0.05; **, P <0.01; ***, P <0.001 (two-way ANOVA with Bonferroni adjustment).

Figure EV3. cPLA$_2$α cooperates with ATGL in mediation of lipid droplet-driven lipid mediator production. (**A**) Quantitative PCR analysis of cPLA$_2$α gene expression in control (SCR) and cPLA$_2$-knockdown (cPLA$_2$α^{KD}) cells grown for 48 h in complete medium and serum starved for 24 h. (**B**) Representative Western blots showing cPLA$_2$α and ATGL protein expression in single and double knockdown A549 cells, without and with hGX sPLA$_2$ pre-treatment, plus basal levels of cPLA$_2$α protein expression in the four cancer cell lines. (**C**) Diagram illustrating the experimental conditions used (top), and changes in neutral lipid content in serum-fed cells induced by ATGL (ATGL^{KD}) and cPLA$_2$α (cPLA$_2$α^{KD}) single and double (Double^{KD}) knockdowns, in comparison with control siRNA-treated cells (SCR), without and with stimulation of lipid droplet biogenesis by hGX sPLA$_2$ treatment. (**D**) Quantitative PCR analysis of cPLA$_2$α gene expression in control (empty) and cPLA$_2$α-overexpressing (cPLA$_2$α^{OE}) cells grown for 48 h in complete medium and serum starved for 24 h. (**E**) Diagram illustrating the experimental conditions used (top), and neutral lipid levels in cells with reciprocal knockdown/ overexpression of cPLA$_2$α and ATGL. Cells were reverse transfected with ATGL-targeting (ATGL^{KD}) and/or cPLA$_2$α-targeting (cPLA$_2$α^{KD}) siRNAs, then forward transfected with ATGL-encoding (ATGL^{OE}) and/or cPLA$_2$α-encoding (cPLA$_2$α^{OE}) plasmids, and/or pre-treated with hGX sPLA$_2$. In controls (control), non-targeting siRNA reverse transfections were combined with backbone ('empty') vector forward transfections. (**F**) Diagram illustrating the experimental conditions used (top), and DGAT inhibition (DGATi)-induced changes in PGE$_2$ production in serum-starved control cells (empty) and in cells overexpressing ATGL (ATGL^{OE}) or cPLA$_2$α (cPLA$_2$α^{OE}), without and with additional stimulation of lipid droplet biogenesis by hGX sPLA$_2$ pre-treatment. Neutral lipid content was quantified by Nile Red staining and flow cytometry. Data are means ±SEM of two (**A**, **D**; **C**, A549 cells) or at least three independent experiments. *, P <0.05; **, P <0.01; ***, P <0.001 (unpaired t-tests (**A, D**); two-way ANOVA with Tukey (**C, E**) or Dunnet (**F**) adjustments).

Figure EV4. cPLA$_2$α affects lipid droplet turnover in Hela and A549 cells. (**A, C**) Representative live-cell confocal microscopy imaging of lipid droplets in ATGL (ATGL^{KD}) and cPLA$_2$α (cPLA$_2$α^{KD}) single and double (Double^{KD}) knockdown HeLa (**A**) and A549 (**C**) cells in comparison with control siRNA-treated cells (SCR), without and with stimulation of lipid droplet biogenesis by hGX sPLA$_2$, treated as shown in Figure 7A. Lipid droplets were stained with BODIPY 493/503 (green) and nuclei with Hoechst 33342 (blue) and images analysed using ImageJ and the Lipid Droplet Counter Plugin. (**B, D**) Box plots and curves showing changes in lipid droplet diameters in cells shown in (A, C), respectively (n >40 cells/sample). Data are geometric means ±SEM (n >40 cells/sample) of two independent experiments. *, P <0.05; **, P <0.01; ***, P <0.001 (nested one-way ANOVA with Sidak adjustment (B, D)).

Figure EV5. Membrane phospholipid PUFA content is modulated by sPLA$_2$, cPLA$_2$α and ATGL. (**A**) Illustration of hypothetical pathways of ATGL-mediated and cPLA$_2$α-mediated modulation of PUFA trafficking between membrane phospholipids and triglycerides (TAGs) stored in lipid droplets. (**B**) Diagram illustrating experimental scheme for the untargeted lipidomic analysis in Figure 7 and (C) and (D). (**C, D**) Untargeted lipidomic analysis of phospholipids in MDA-MB-231 cells depleted of ATGL (ATGL^{KD}), cPLA$_2$α (cPLA$_2$α^{KD}) or both (Double^{KD}), without and with hGX sPLA$_2$ pre-treatment, and grown as shown in (B). Volcano plots show significant changes (–log$_{10}$(P value) >1.30) in individual lipids between each treatment condition *versus* control cells (unless otherwise indicated), and were prepared by log$_2$ fold-change (FC) data transformation and multiple t-test analysis (n=3 independent experiments). Phospholipids (PLs) containing saturated and mono-unsaturated acyl chains (SFA/MUFA-PLs with 0–2 double bonds) and those containing polyunsaturated FAs (PUFA-PLs with at least 3 double bonds) are colour-coded as indicated. PC, phosphatidylcholine; PE, phosphatidylethanolamine; PI, phosphatidylinositol, PS, phosphatidyserine.

Appendix Figure Legends

Appendix Figure S1. $sPLA_2$-induced changes in lipid droplet metabolism and composition. (**A**) Total cellular triglycerides (TAGs) in control and hGX-$sPLA_2$-treated MDA-MB-231 and HeLa cells quantified using a biochemical assay. (**B, C**) Diagram illustrating the experimental set-up for oleate incorporation analyses using thin layer chromatography (TLC) shown in (**C**) and in Figure 1D. (**C**) Representative TLC plate showing that in hGX-$sPLA_2$-treated cells, oleate is preferentially incorporated into TAGs, but not into phosphatidylcholine (PC) or cholesterol esters (CE). (**D, E**) Lipidomic analysis of hGX-$sPLA_2$-induced PUFA-TAG enrichment in MDA-MB-231 cells grown under serum-rich conditions. (**D**) Representative XY z-score plot showing colour-coded changes in the levels of TAG acyl-chain unsaturation. Data are means ±SEM of two (**A**) and four (**E**) independent experiments. *, P <0.05; **, P <0.01; ***, P <0.001 (two-way ANOVA with Bonferroni adjustment (**A**); unpaired t-tests (**E**)).

Appendix Figure S2. Depletion of ATGL suppresses both basal and hGX-$sPLA_2$-stimulated lipid mediator production in breast cancer cells. hGX-$sPLA_2$-induced and ATGL knockdown ($ATGL^{KD}$)-induced changes in selected lipid mediators (as indicated) released from serum-starved MDA-MB-231 cells. Cells were treated as shown in Figure 3A. Data are means ±SEM of three independent experiments. *, P <0.05; **, P <0.01; ***, P <0.001 (two-way ANOVA with Sidak adjustment). EPA, eicosapentaenoic acid; HEPE, hydroxyeicosapentaenoic acid; AA, arachidonic acid; TXB_2, thromboxane B_2; PD1, protectin D1; AT-PD1, aspirin-triggered protectin D1; MaR1, maresin 1; RvD2, resolvin D2; RvD3, resolvin D3; RvD4, resolvin D4.

Appendix Figure S3. LION-term enrichment analysis for significant changes in membrane properties induced by $sPLA_2$, $cPLA_2\alpha$ and ATGL. (**A**) Heat map of z-score scaled lipid levels of phospholipids and triglycerides in serum-starved MDA-MB-231 cells depleted of ATGL ($ATGL^{KD}$), $cPLA_2\alpha$ ($cPLA_2\alpha^{KD}$) or both ($Double^{KD}$), without and with hGX $sPLA_2$ pre-treatment under serum-rich conditions, and grown as shown in Figure EV5B. (**B, C**) LION-term enrichment analysis of the full data set (B) and pairwise comparisons of phospholipid data from $cPLA_2\alpha$-depleted and control (SCR) cells (C) in ranking mode. The cut-off value of significant enrichments is indicated by the grey line (q <0.05). Data were analysed using three principal components, and lipids were clustered into five groups by hierarchical clustering (A, B). Bar colours are scaled according to the enrichment (−log q-values). FDR, false-discovery rate.

Figure 1

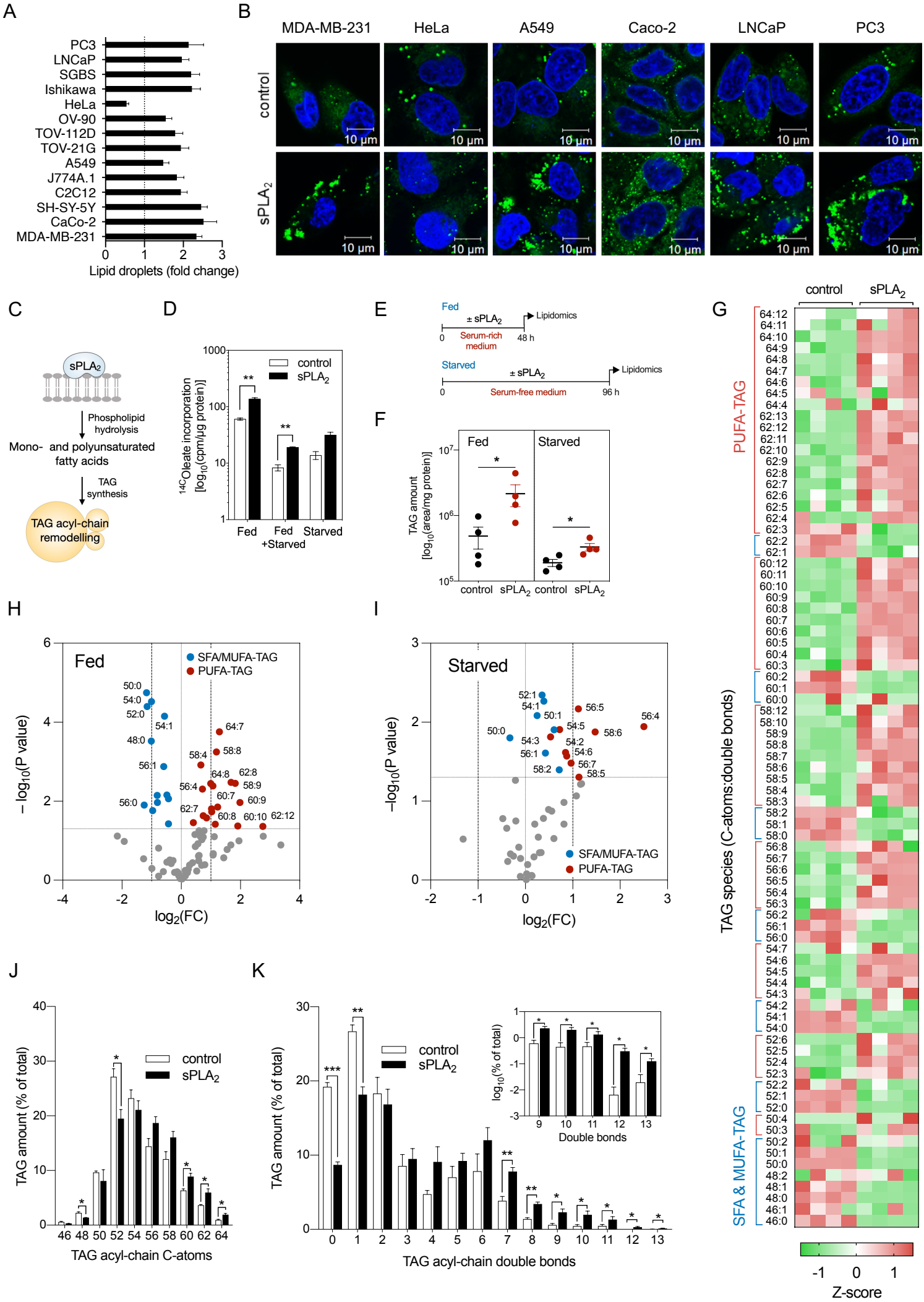

Figure 2

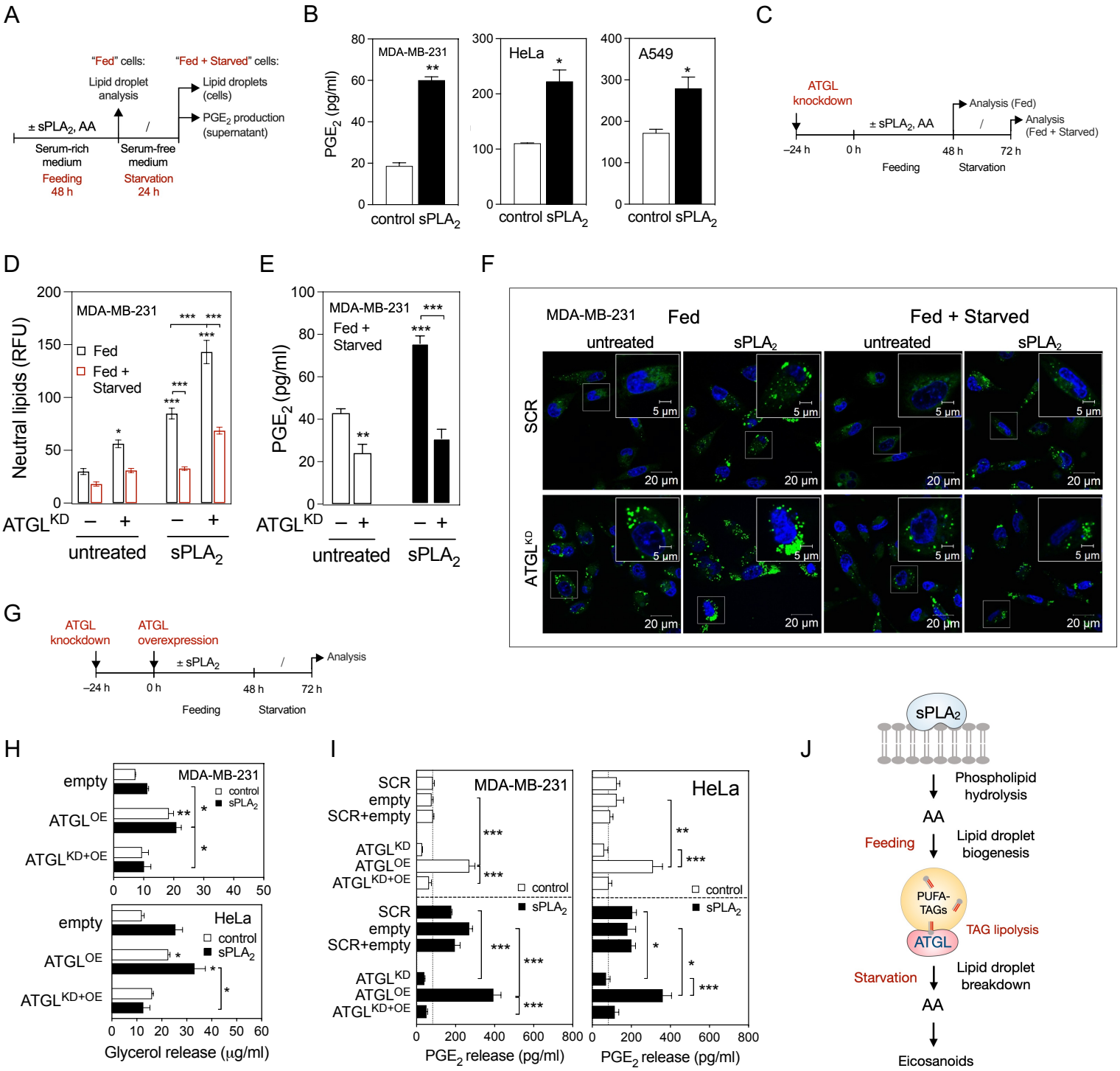

Figure 3

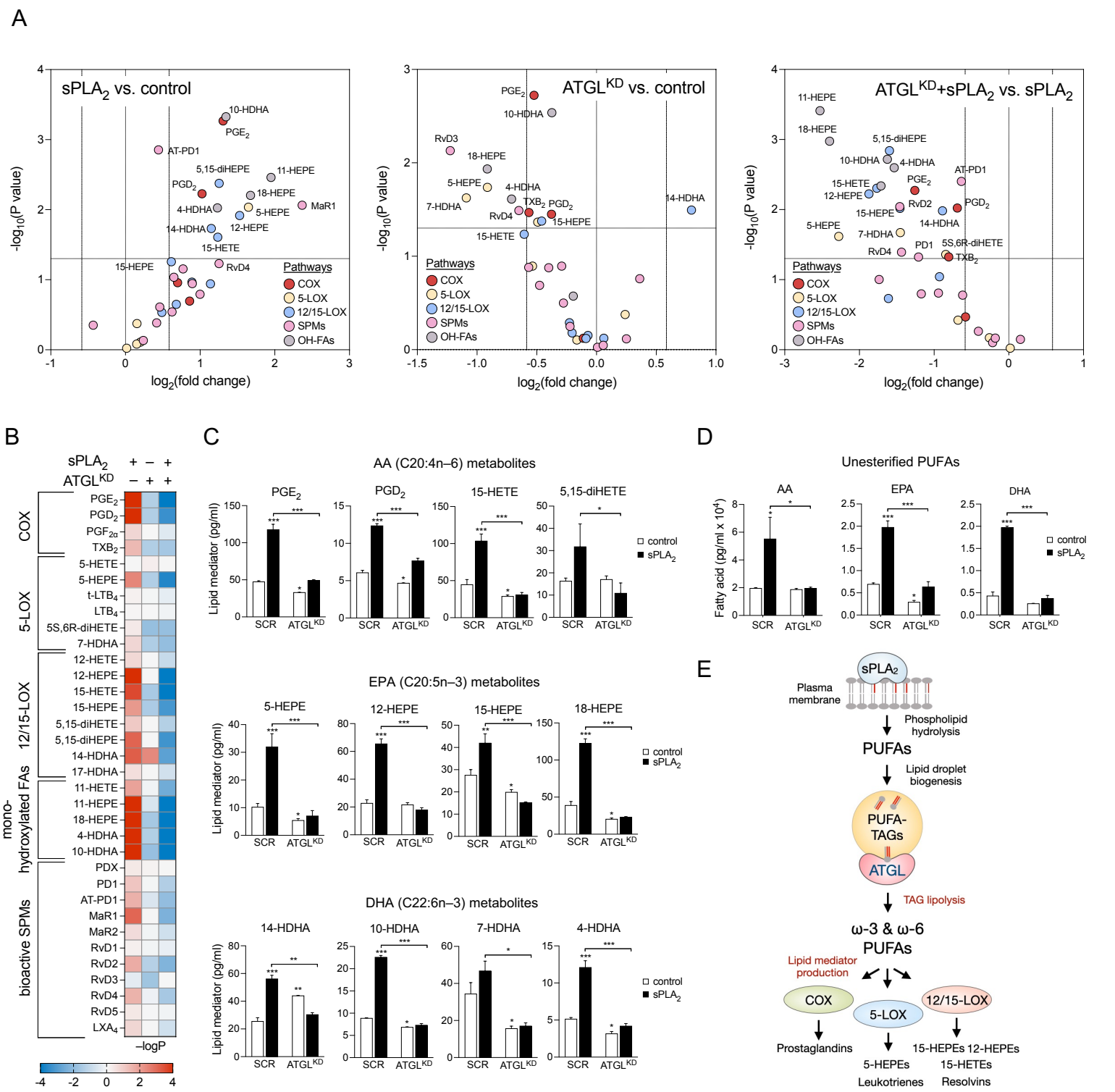

Figure 4

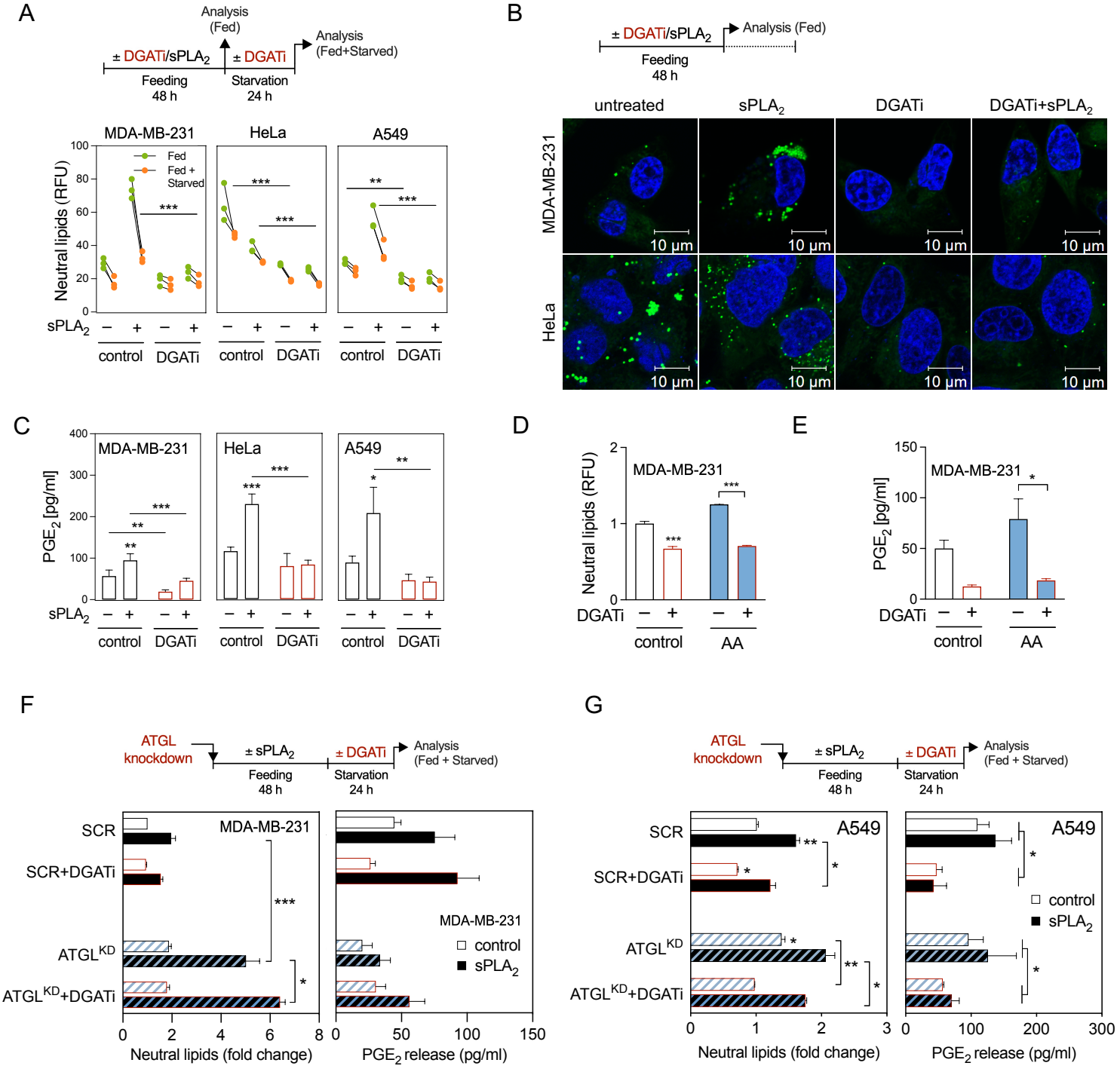

Figure 5

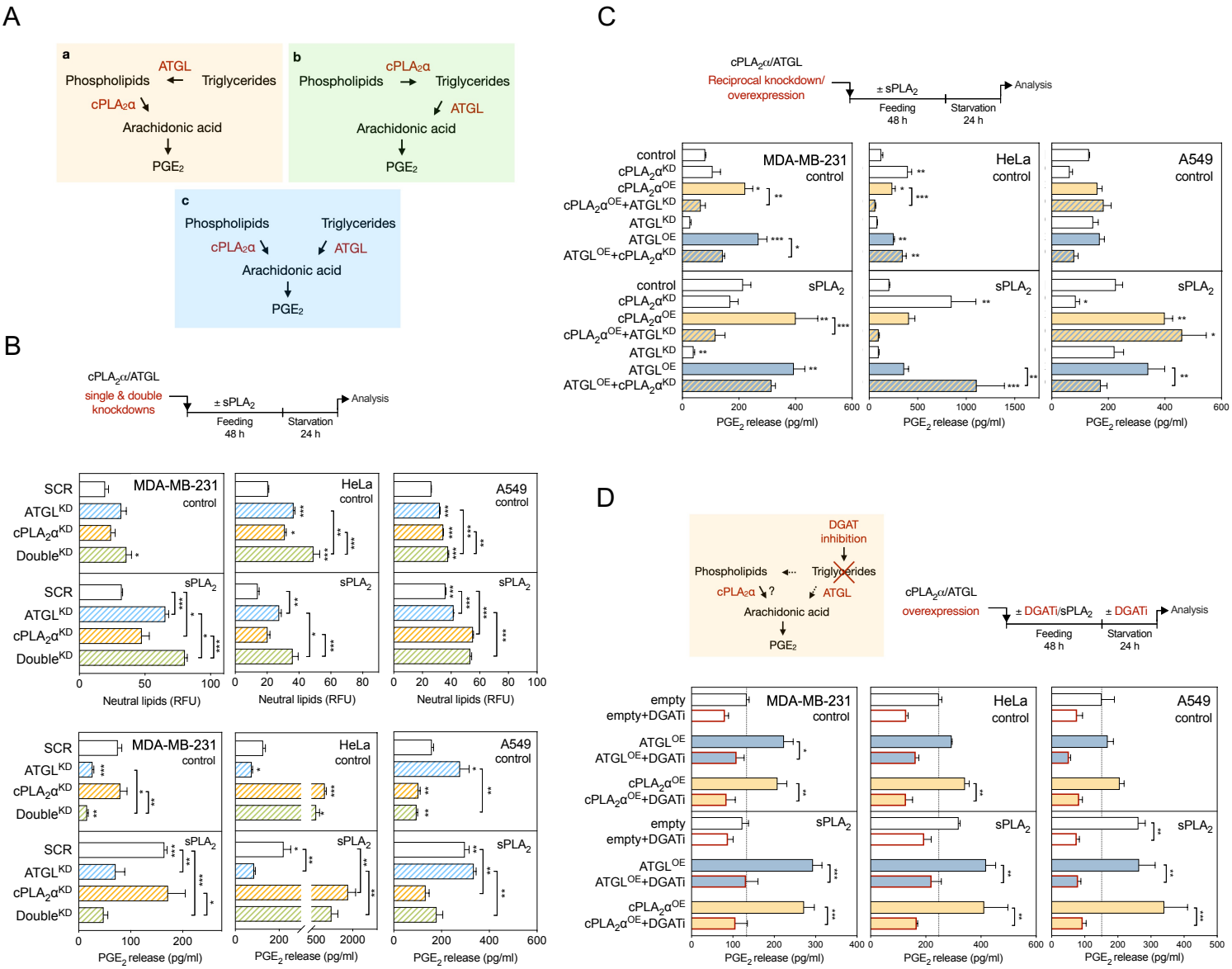

Figure 6

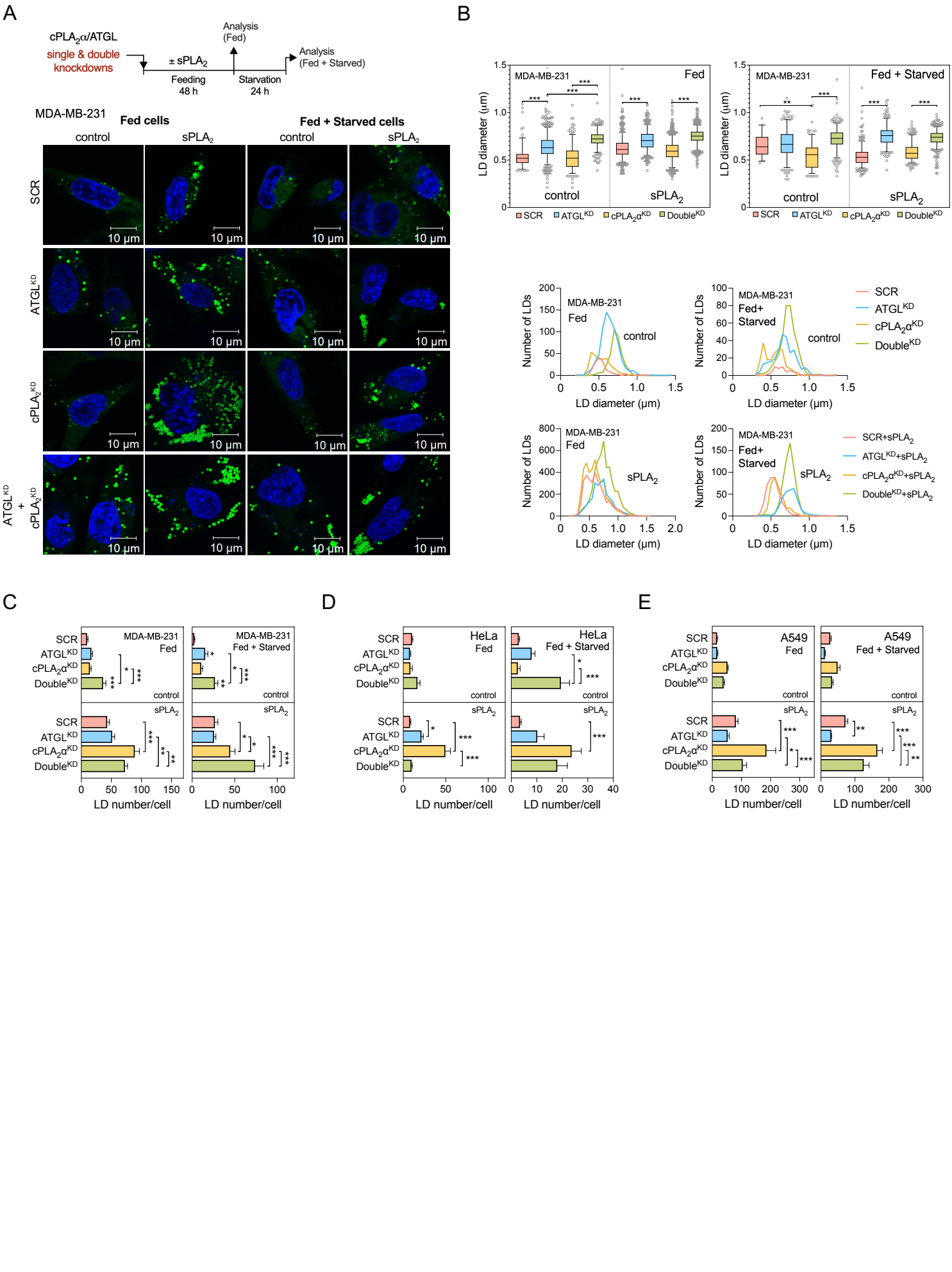

Figure 7

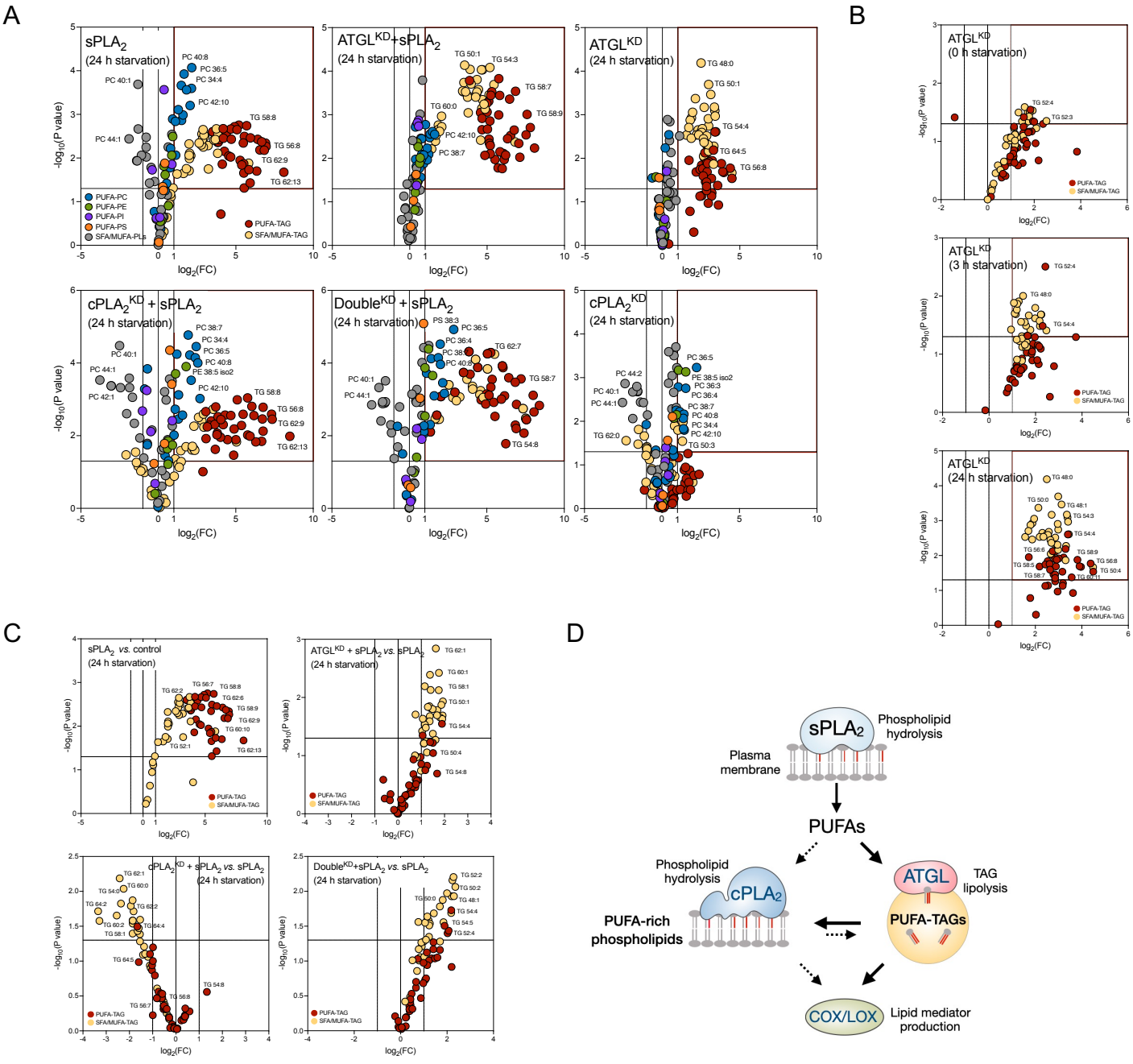

Figure 8

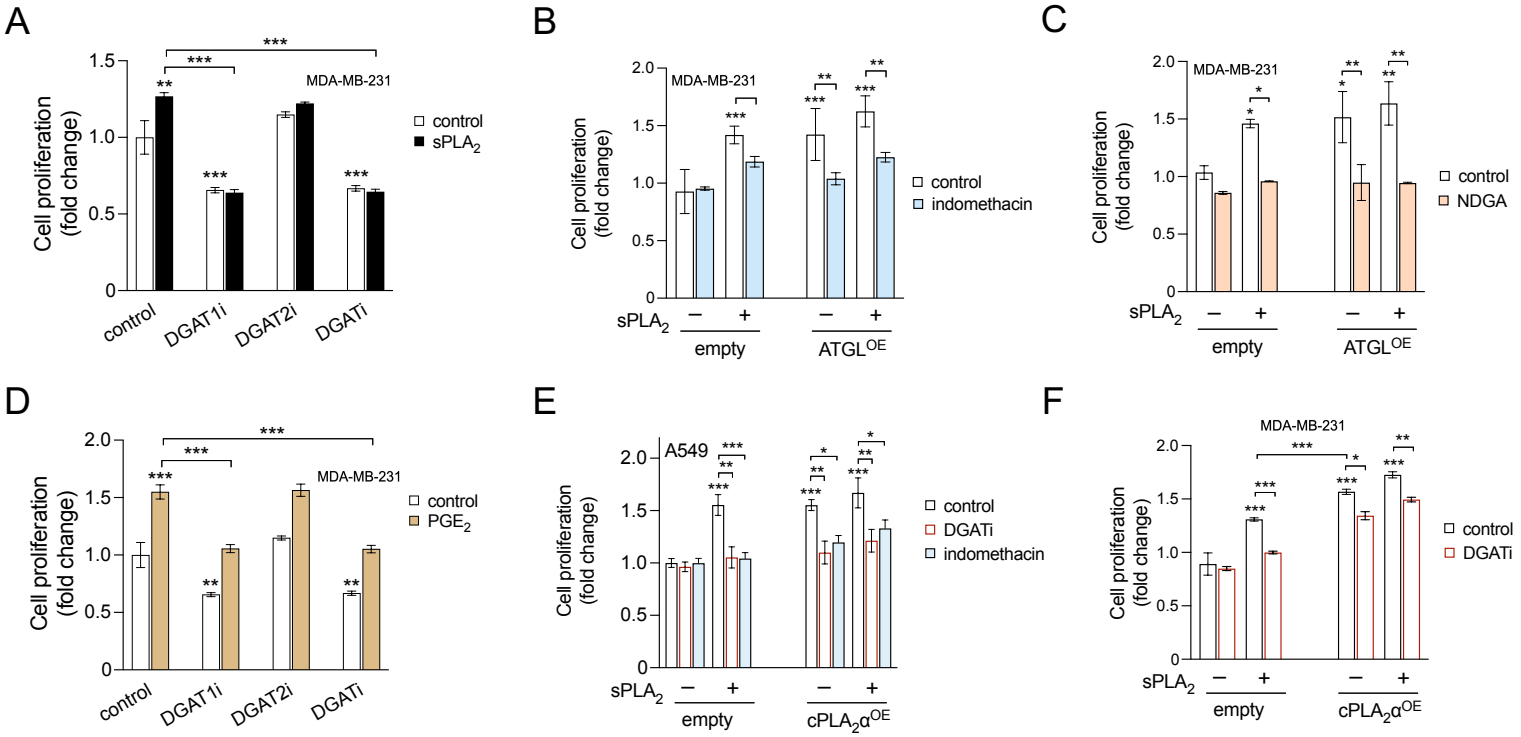

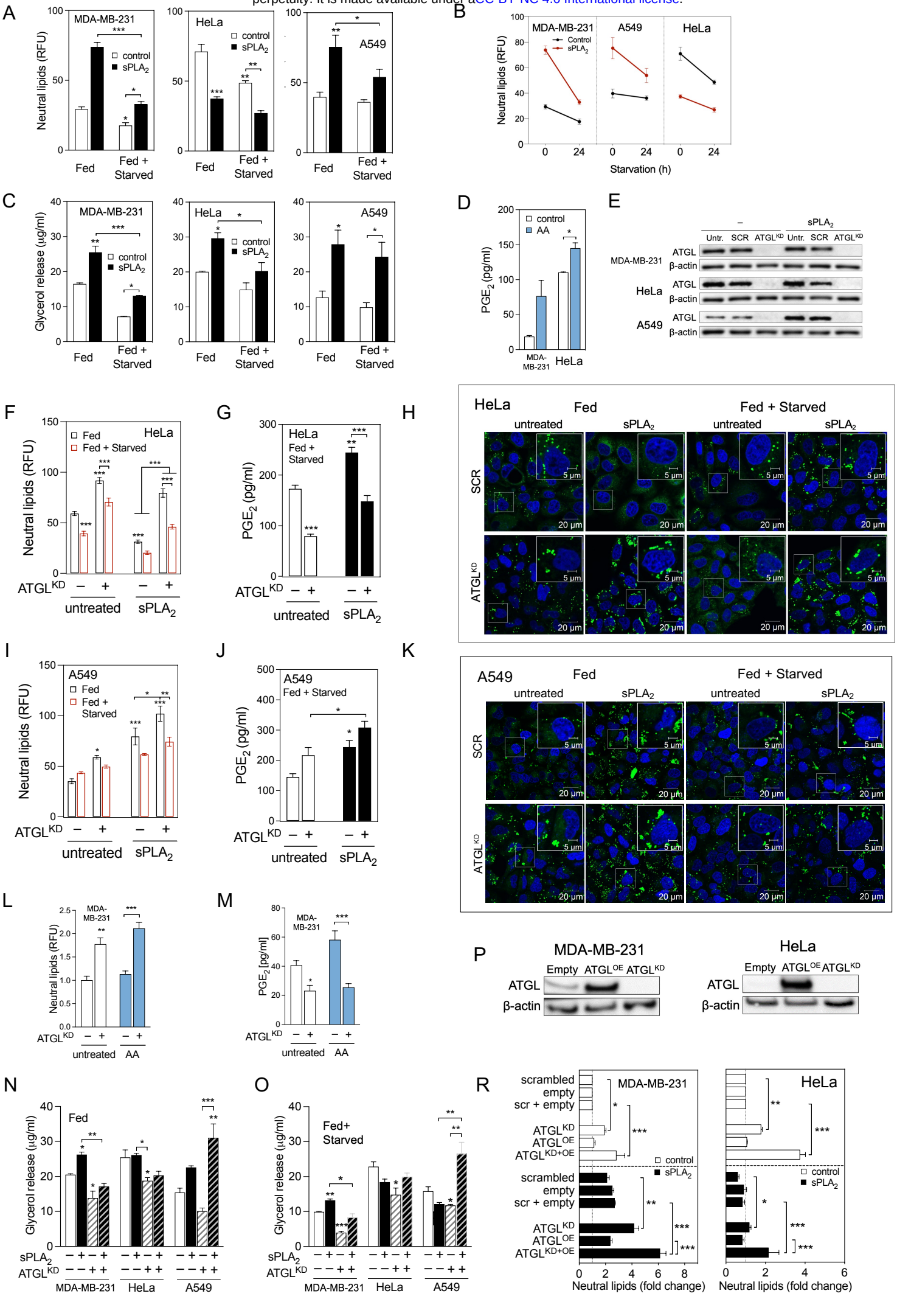

A

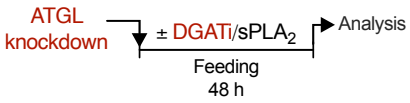

B

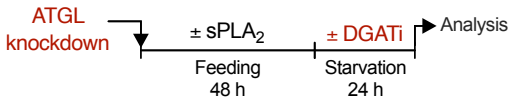

MDA-MB-231

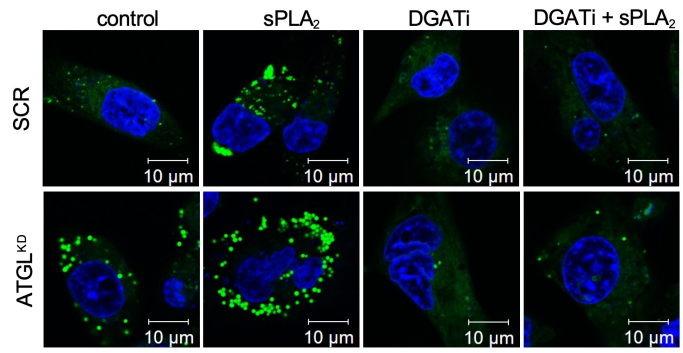

MDA-MB-231

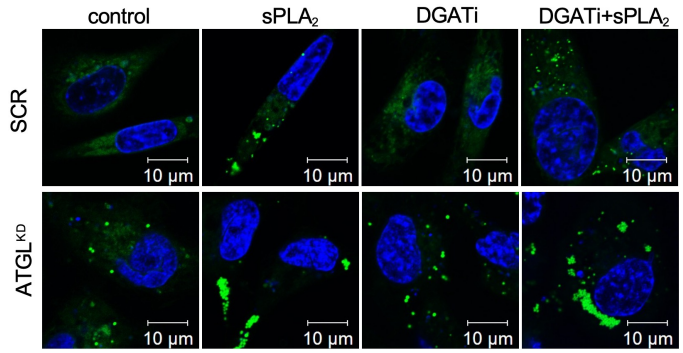

HeLa

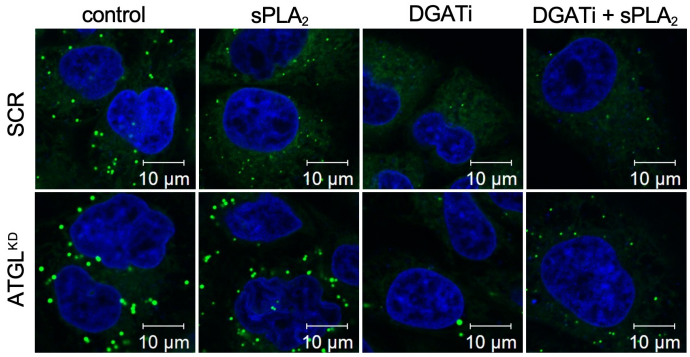

HeLa

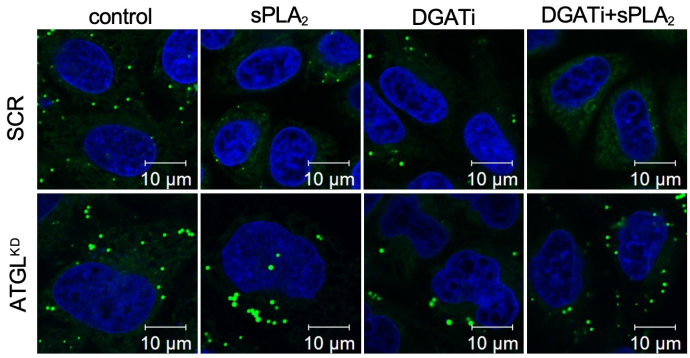

C

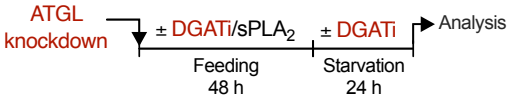

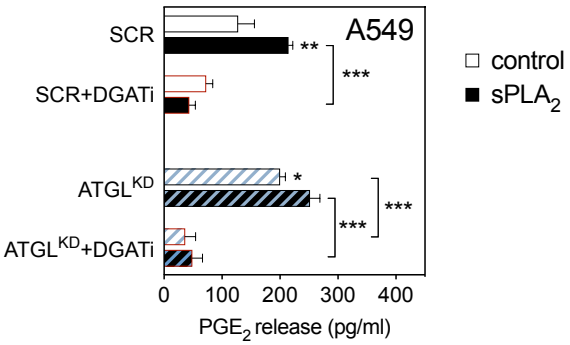

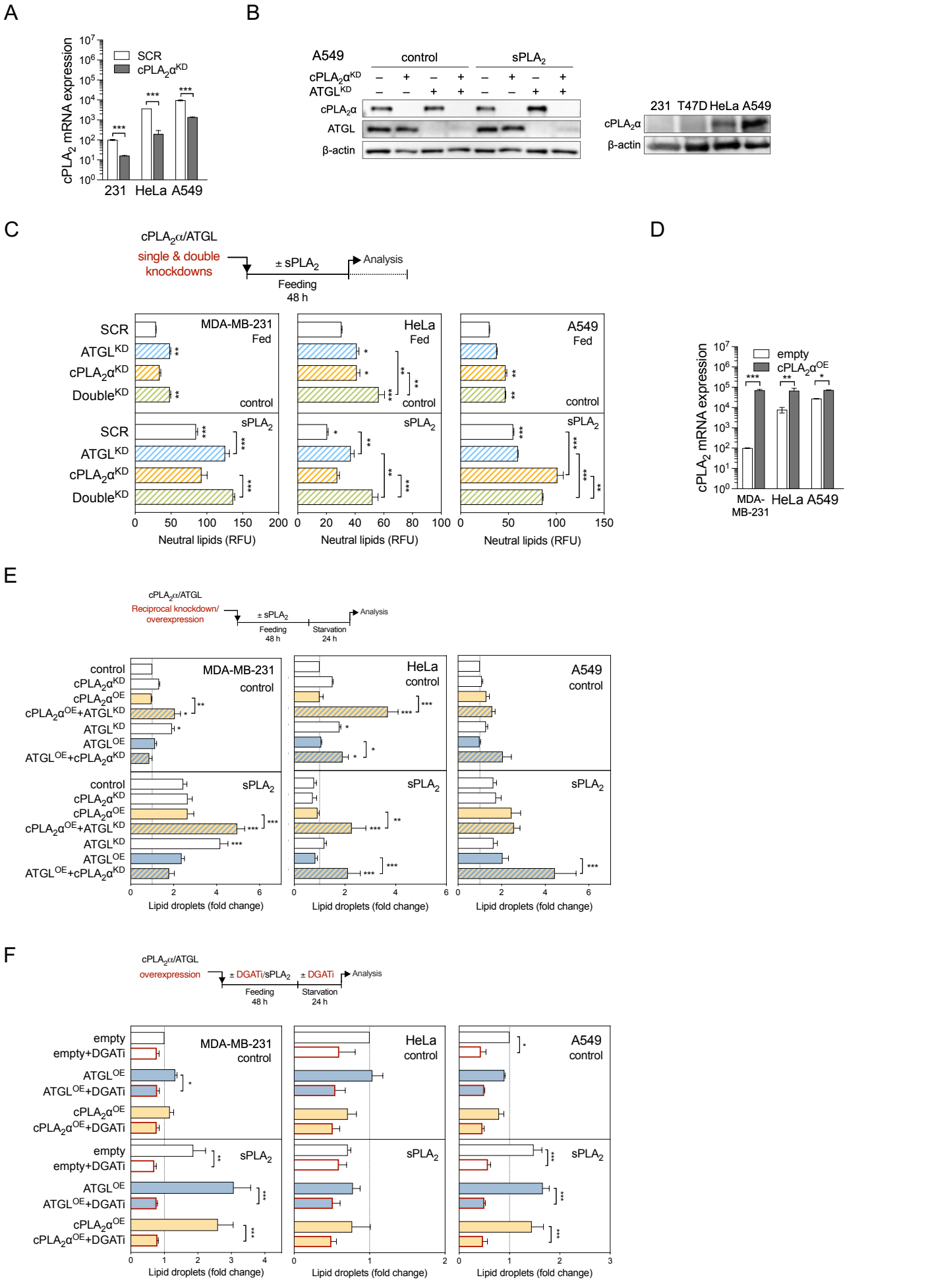

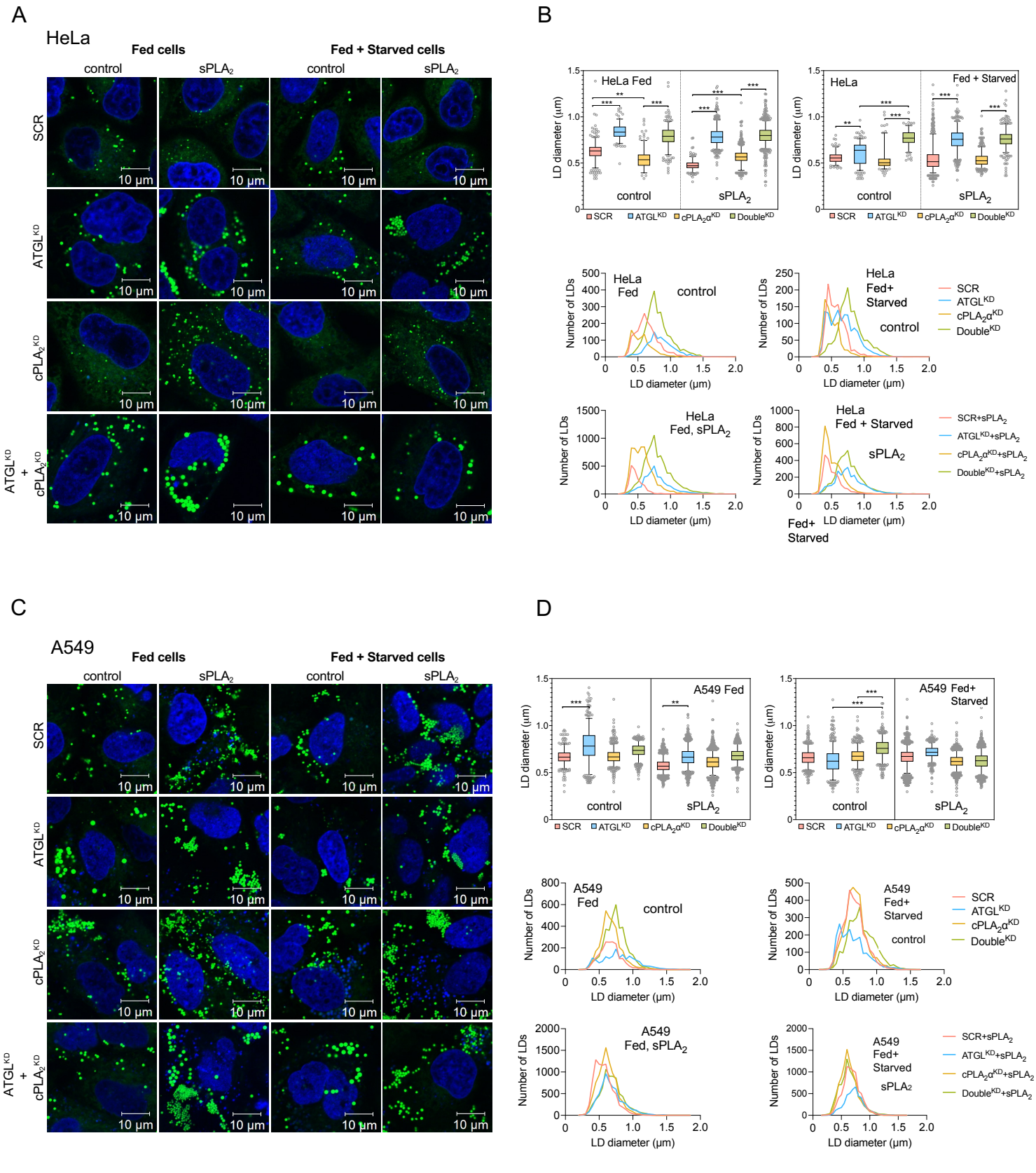

Figure EV5

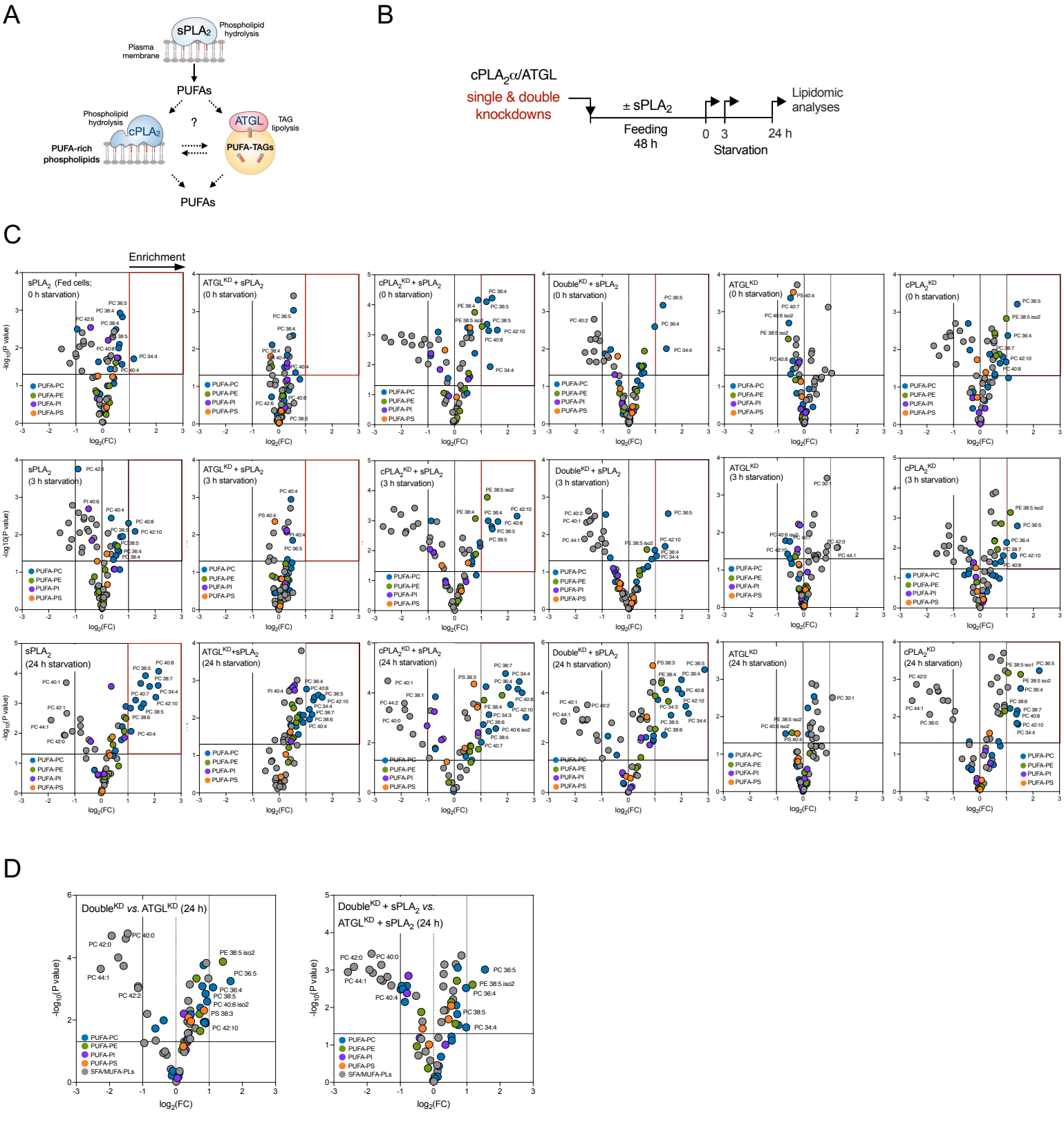

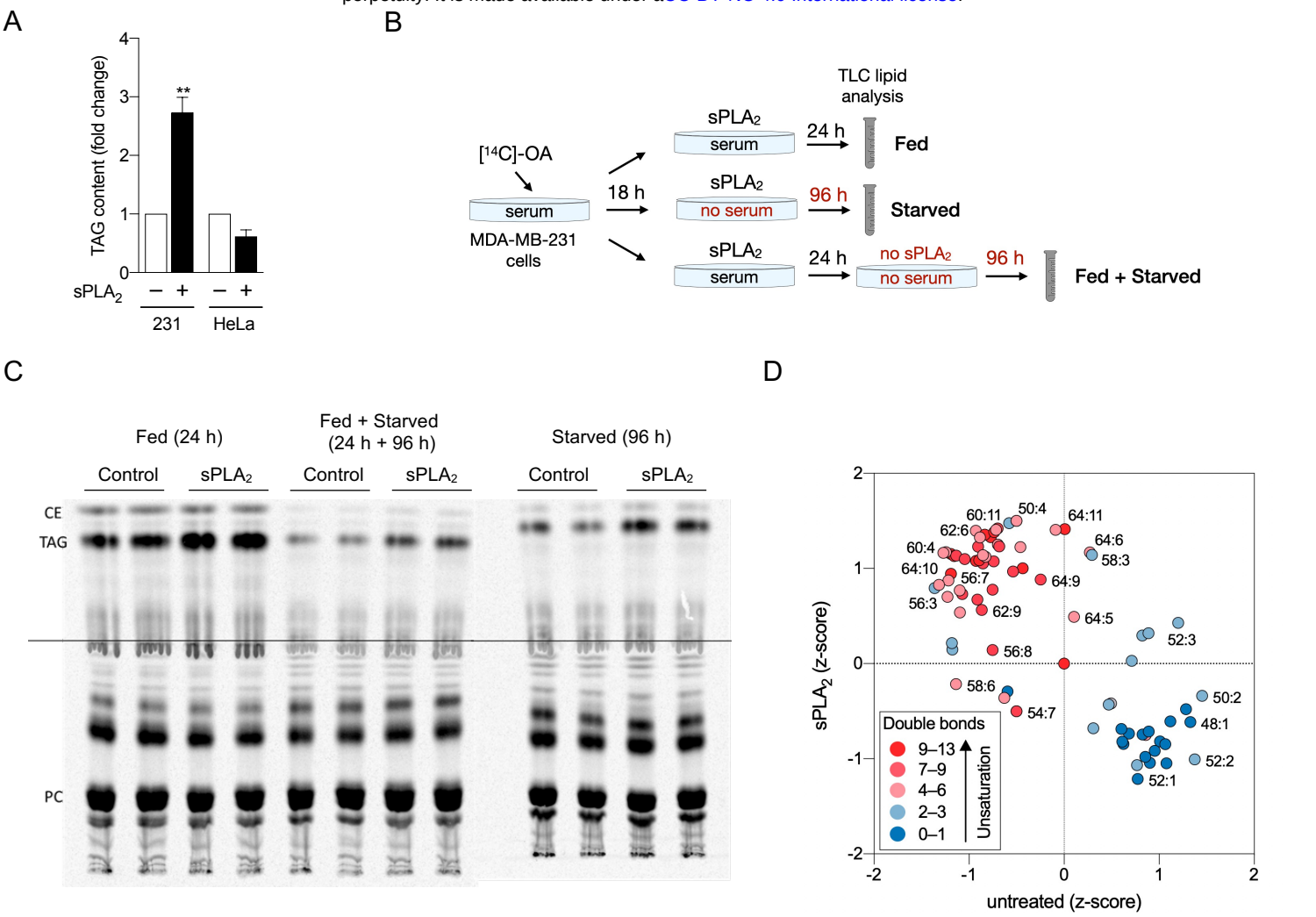

EPA metabolites

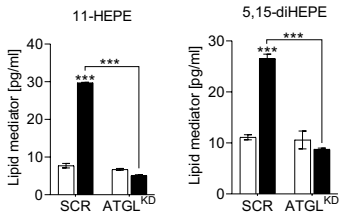

AA metabolites

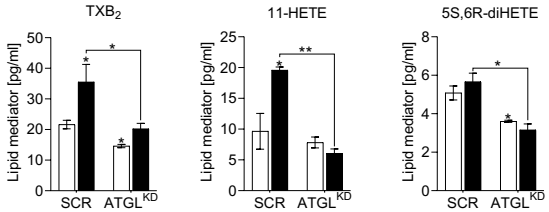

DHA metabolites

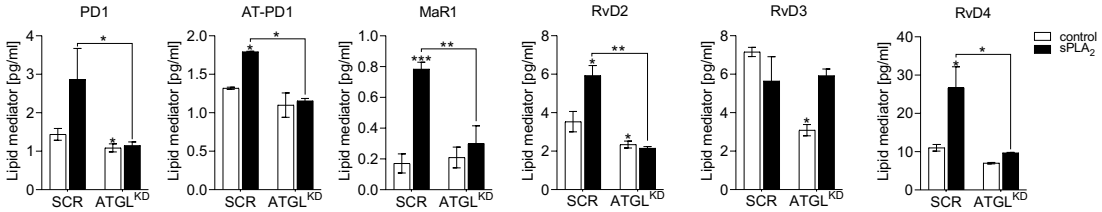

A

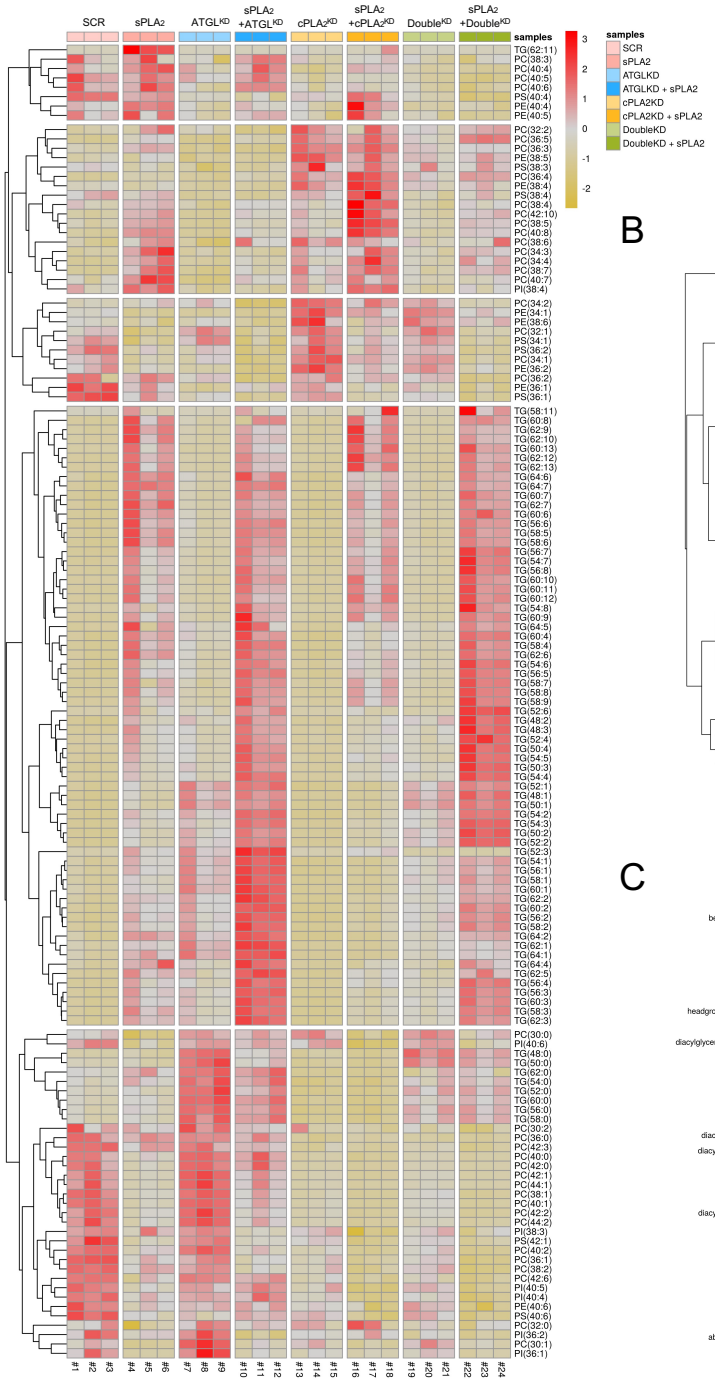

B

C